Molecular Therapy
Methods & Clinical Development
Original Article

AAV-S: A versatile capsid variant for transduction of mouse and primate inner ear

Maryna V. Ivanchenko,[1,4] Killian S. Hanlon,[1,2,4] Daniel M. Hathaway,[1] Alex J. Klein,[1] Cole W. Peters,[1] Yaqiao Li,[1] Panos I. Tamvakologos,[1] Josette Nammour,[2] Casey A. Maguire,[2,3] and David P. Corey[1]

[1]Department of Neurobiology, Harvard Medical School, 220 Longwood Avenue, Boston, MA 02115, USA; [2]Molecular Neurogenetics Unit, Massachusetts General Hospital, 13th Street, Charlestown, MA 02114, USA; [3]Department of Neurology, Harvard Medical School, 25 Shattuck Street, Boston, MA 02115, USA

Gene therapy strategies using adeno-associated virus (AAV) vectors to treat hereditary deafnesses have shown remarkable efficacy in some mouse models of hearing loss. Even so, there are few AAV capsids that transduce both inner and outer hair cells—the cells that express most deafness genes—and fewer still shown to transduce hair cells efficiently in primates. AAV capsids with robust transduction of inner and outer hair cells in primate cochlea will be needed for most clinical trials. Here, we test a capsid that we previously isolated from a random capsid library, AAV-S, for transduction in mouse and non-human primate inner ear. In both mice and cynomolgus macaques, AAV-S mediates highly efficient reporter gene expression in a variety of cochlear cells, including inner and outer hair cells, fibrocytes, and supporting cells. In a mouse model of Usher syndrome type 3A, AAV-S encoding CLRN1 robustly and durably rescues hearing. Overall, our data indicate that AAV-S is a promising candidate for therapeutic gene delivery to the human inner ear.

INTRODUCTION

Hereditary hearing loss (HHL) is caused by defects in over 200 genes[1] and affects a variety of cell types in the inner ear. Most of the genes mutated in HHL are expressed by the inner and outer hair cells (IHCs, OHCs), the sensory cells of the cochlea,[2] and so effective AAV vectors employed for therapeutic gene delivery must target both of these cell types. The first gene therapy studies in the ear involved a limited number of capsids, most notably adeno-associated virus (AAV)1.[3,4] However, AAV1 primarily targets IHCs and not OHCs, whereas both are required for functional hearing. In more recent years, several groups, including our own, have developed AAV-based vectors that can efficiently transduce both IHCs and OHCs.[5–9] Mutations in genes expressed by spiral ganglion neurons (SGNs), supporting cells, and fibrocytes also cause HHL. In fact, the most common form of HHL, DFNB1, is caused by mutations in *GJB2*, expressed in fibrocytes and supporting cells of the cochlea. Thus, AAV capsids that can deliver genetic payloads to a variety of clinically relevant cell types are greatly needed.

Most studies of gene therapy for HHL have involved vector delivery to the inner ears of neonatal mice. However, it is difficult to predict whether transgene delivery by any specific AAV in a neonatal mouse inner ear will translate to infant or adult human cochlea, and there have been notable instances of AAV vectors failing to translate to human. Parallel testing in non-human primates (NHPs) is thus critically important.

Recently, we reported a method for selecting potent vectors from a random peptide display capsid library and used that to select AAV9 vector variants capable of transducing the brain after intravenous delivery.[10] Of the two variants studied in this work, one (AAV-F) proved highly successful with systemic delivery, while the other (AAV-S) failed to effectively penetrate the blood-brain barrier. However, AAV-S efficiently transduced peripheral organs and mediated high expression of a reporter gene when directly injected into the brain. We hypothesized that the unique AAV-S peptide insertion might also enable effective transduction of the inner ear.

Here, we demonstrate that AAV-S is a highly potent vector for driving expression in the inner ears of both mice and NHPs. In the inner ears of mice, we found that AAV-S transduces a wide variety of cell types, including IHCs and OHCs. We evaluated the ability of AAV-S to express genes in the inner ears of cynomolgus monkeys and found widespread expression throughout the cochlea, in both IHCs and OHCs as well as in cell types relevant to deafnesses, such as DFNB1. We also tested the AAV-S capsid for delivery of a therapeutic gene in a mouse model of Usher syndrome type 3A. Usher 3A is caused by mutations in *CLRN1*; the mouse model (TgAC1/Clrn1-KO) has late-onset disruption of the *Clrn1* gene. AAV-S delivering a codon-optimized Clrn1 expression cassette to the inner ear provided significant protection against loss of hearing, with rescue to wild-type levels in low and middle frequencies, which was durable for at least 5 months post-injection. Further, scanning electron microscopy and immunofluorescence of treated and untreated mouse cochleas showed that cell

Received 17 January 2021; accepted 24 March 2021;
https://doi.org/10.1016/j.omtm.2021.03.019.

[4]These authors contributed equally

Correspondence: Casey A. Maguire, Molecular Neurogenetics Unit, Massachusetts General Hospital, 13th Street, Charlestown, MA 02114, USA.
E-mail: cmaguire@mgh.harvard.edu
Correspondence: David P. Corey, Department of Neurobiology, Harvard Medical School, 220 Longwood Avenue, Boston, MA 02115, USA.
E-mail: dcorey@hms.harvard.edu

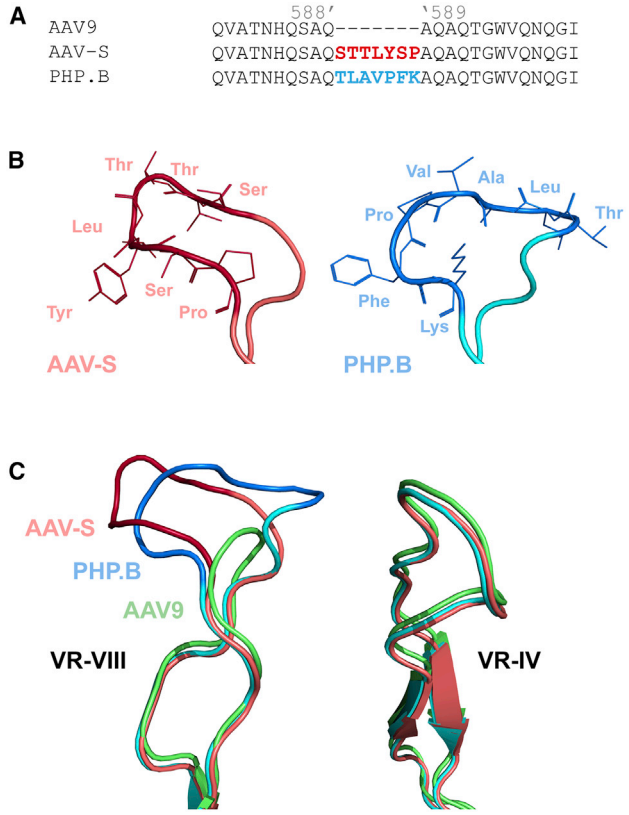

Figure 1. The AAV-S peptide is unlikely to distort capsid protein structure
(A) Insertion point of AAV-S peptide in variable region VIII (VR-VIII) of the AAV9 capsid protein, with PHP.B insertion shown for comparison. (B) Peptide loop of AAV-S and PHP.B inserts. The structure of AAV9 VP3 (PDB: 3UX1) was modified with AAV-S or PHP.B residues and modeled using SWISS-MODEL to assess likely conformations of variants. (C) AAV-S and PHP.B loops in the context of VR-VIII, with AAV9 inset, modeled by SWISS-MODEL. Insertion is not predicted to affect capsid protein structure outside of VR-VIII, including the nearby VR-IV.

numbers were maintained and hair-cell bundle morphology was preserved in treated animals. Overall, we show that AAV-S is a powerful new vector for targeting the inner ears of both rodents and primates and can serve as both an effective research tool and a promising candidate for treatment of human HHL.

RESULTS

Protein modeling suggests that the AAV-S peptide insertion in the variable region VIII (VR-VIII) loop of the AAV capsid is unlikely to disrupt structure

We previously identified an AAV9 capsid variant, AAV-S, in a screen for variants that could efficiently target the brain.[10] While AAV-S did not effectively pass the blood-brain barrier, it was highly efficient at targeting peripheral organs. AAV-S contains a 7-amino-acid insert (STTLYSP) between positions 588 and 589 of the AAV9 VP1 capsid protein (Figure 1A). This is the same location as the unique insert in AAV9-PHP.B (TLAVPFK), another variant selected in brain that can efficiently transduce cells in the inner ear. As crystal structures for these variants are unavailable, we used SWISS-MODEL to model the effect of the insertion on the structure of the viral capsid protein (Figure 1B). As expected, the insertions into the VR-VIII loop do not seem to have a dramatic effect on the protein structure outside of the insertion point. Both AAV-S and AAV9-PHP.B peptides are predicted to form a short loop extending from VR-VIII, but not to affect the structure of the rest of the protein (VR-IV is shown as an example in Figure 1C). The AAV-S peptide shares some similarity with PHP.B (a single proline and an aromatic residue), but the AAV-S peptide is more polar (STT..S) than that of PHP.B (T…..K), while the lysine in PHP.B confers a positive charge that AAV-S lacks.

The AAV-S capsid mediates efficient transgene expression in a variety of cell types in the mouse inner ear

Because AAV-S targets a variety of cell types,[10] we wondered if it would transduce cells in the mammalian inner ear. To gauge the efficacy of AAV-S, we first injected cochleas of wild-type C56BL/6J mice with the vector expressing EGFP under the control of the chicken beta actin (CBA) promoter (AAV-S-CBA-EGFP; Figure S1A). At postnatal day 1 (P1), mice were injected with 3×10^{10} vector genomes (VG) via the round window membrane (RWM). At P6, cochleas were dissected, immunostained, and imaged (Figure 2). Overall, we found high levels of transduction throughout the inner ear with AAV-S-CBA-EGFP. In the organ of Corti, a majority of hair cells were transduced, with nearly 100% of IHCs and well over half of OHCs expressing EGFP (Figures 2B, 2I, and 2I′). OHC expression varied from apex to base, with ~75% of apical OHCs transduced (reaching up to 100%) versus ~50% of basal OHCs. A similar gradient has been observed for a number of different AAV vectors.[4,5,9] The modest transduction in basal OHCs is unlikely to be a consequence of limited vector diffusion, because the basal turn of the cochlea is nearest the injection site and because labeled cells were observed throughout the inner ear. It might reflect a gradient in a capsid receptor or in promoter efficacy.

Aside from hair cells, AAV-S targeted many cell types in the cochlea. In neonatal mice, nerve fibers of SGNs from apex to base were labeled with EGFP (Figure 2C), as well as SGN cell bodies (Figure 2D) as confirmed by co-labeling for the neuronal marker neurofilament H (NF-H). Interestingly, we observed transduction in supporting cells, in interdental cells, and in fibrocytes of the spiral limbus (Figure 2E) and lateral wall (Figure 2F), as well as consistent expression in inner and outer sulcus cells and Claudius cells (Figures 2G and 2H). However, we saw little if any GFP expression in Hensen's cells.

Since the perilymph of the cochlea is continuous with that of the vestibular organs, we expected that RWM injection would be a suitable delivery route for targeting vestibular hair cells. Analysis of whole-mount saccular macula samples revealed a wide array of type I and type II hair cells, as well as supporting cells transduced within this vestibular organ (Figures 2J and 2J′), further highlighting the efficiency of AAV-S.

To determine whether vector transduction with AAV-S-CBA-EGFP disrupts auditory function, we measured the auditory brainstem

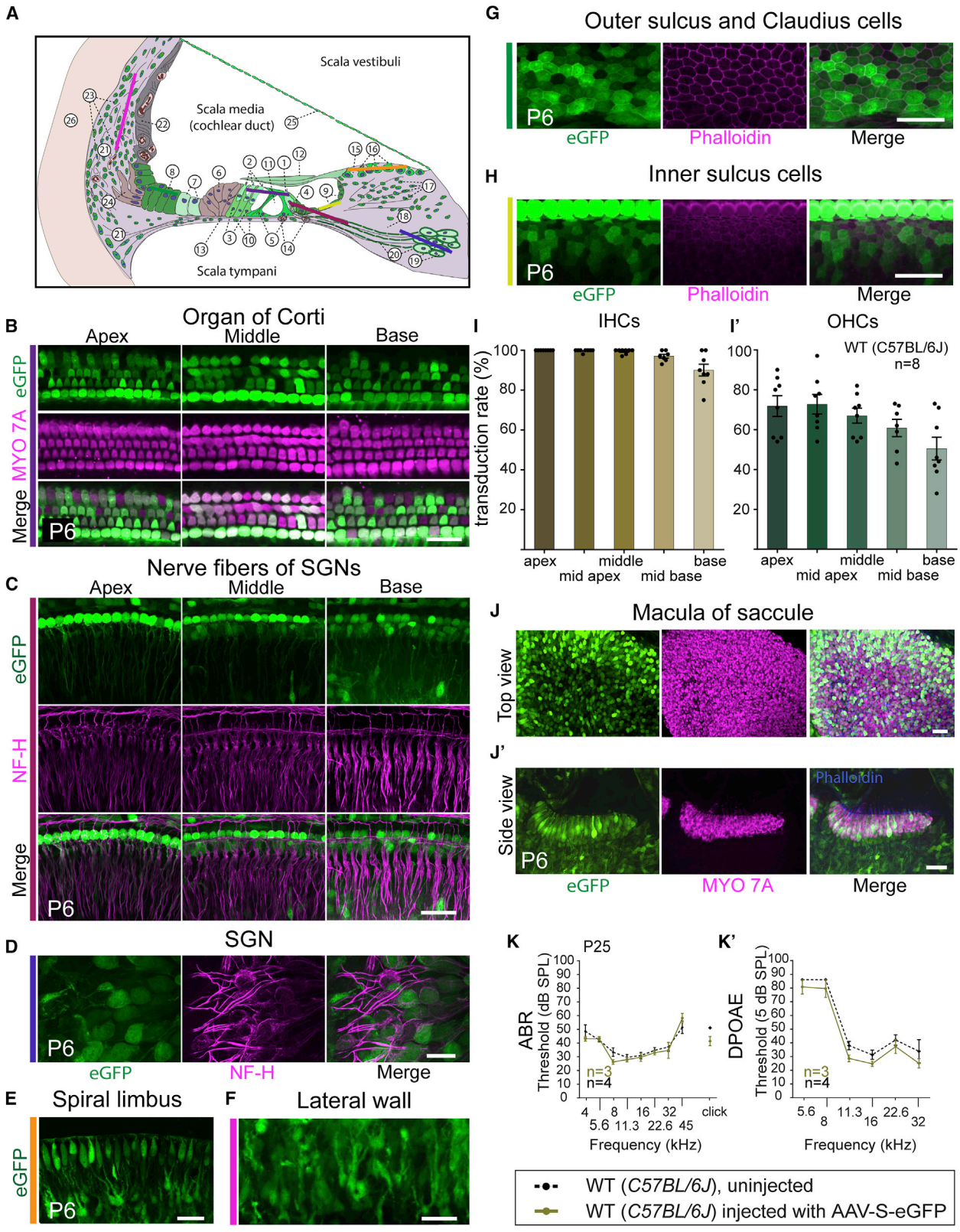

(legend on next page)

response (ABR) and distortion product otoacoustic emissions (DPOAEs) at P25 in mice that received 3×10^{10} VG of AAV-S-CBA-EGFP at P1. Only mice with confirmed cochlear expression of EGFP were included in the ABR and DPOAE analysis. We found no significant differences in ABR or DPOAE thresholds for any frequency relative to uninjected wild-type mice, confirming that AAV-S-mediated EGFP expression did not affect hearing function (Figures 2K and 2K′).

While high-level transduction of the inner ear can be achieved in neonatal mice, it is often much more challenging in adult mice. To test the efficacy of AAV-S, adult mice were injected with 3×10^{10} VG via the posterior semicircular canal (PSC), and the inner ear was dissected, immunostained, and mounted at P42 (Figure S2). We observed broad transduction of AAV-S-CBA-EGFP. IHCs were as effectively transduced as in other studies,[5,11,12] but while most OHCs were transduced, expression levels were extremely weak (Figure S2A). There was no detectible transduction in supporting cells of the organ of Corti.

We also analyzed images of whole mounts immunostained for the neuronal marker NF-H and observed high transduction in satellite glial cells of SGNs and fibrocytes, but not in SGNs and nerve fibers of SGNs (Figures S2B and S2B′). A high level of EGFP expression also was detected in hair cells and supporting cells throughout the saccule and utricle (Figures S2C and S2C′).

AAVS-CBA-optiClrn1 mediates robust and durable rescue of hearing in the *TgAC1+/ClrnKO* mouse model of Usher 3A

In order to gauge the clinical relevance of AAV-S-mediated transgene delivery, we sought to test a therapeutic construct in a mouse model of deafness. Usher syndrome type 3A is caused by recessive mutations in the *CLRN1* gene, encoding the small four-pass transmembrane protein clarin-1, and features a relatively late onset of symptoms, with deafness developing as late as the second decade of life. We used a homozygous *Clrn1* knockout mouse model ($Clrn1^{KO/KO}$) that also incorporates a transgene that transiently expresses *Clrn1* under the control of the *Atoh1* promoter ($TgAC1^{+}$). By delaying the loss of CLRN1, this mouse more accurately mimics the phenotype in humans.[13] We packaged into AAV-S a mouse codon-optimized *Clrn1* coding sequence flanked by 5′ and 3′ UTRs, under the control of the CBA promoter (optiClrn1; Figure S1B).

We injected knockout mice carrying the transgene ($TgAC1^{+}/ClrnKO$) at P1 with 1.9×10^{10} VG of AAV-S-optiClrn1 and assayed their ability to hear at ages P30, P60, P90, P120, and P150 (Figures 3A and 3B). The untreated $TgAC1^{+}/Clrn1KO$ mice progressively lost hearing and were deaf (threshold above 85 dB, the highest tested) by P90. In treated mice, we found a striking rescue of hearing when tested with both ABR and DPOAE (Figures 3A and 3B). ABR showed that $TgAC1^{+}/Clrn1KO$ mice treated with AAV-S-optiClrn1 had hearing as sensitive as wild-type mice at low and middle frequencies. This rescue persisted to P150 (Figure 3A). Hearing at a high frequency (22.6 kHz) was significantly better in treated than in untreated $TgAC1^{+}/Clrn1KO$ up to P90 (Figure 3A). DPOAEs showed a similar pattern, with robust rescue across all frequencies at P30–P90 and a weakening at high frequencies at age P120–P150 (Figure 3B). DPOAE amplitude measured at a representative midrange frequency (11.3 kHz) showed rescue to wild-type level in $TgAC1^{+}/Clrn1KO$ mice treated with AAV-S-optiClrn1, while untreated $TgAC1^{+}/Clrn1KO$ mice had no detectable DPOAEs (Figure S3). Wild-type mice injected with AAV-S-optiClrn1 showed no difference in ABR or DPOAE when compared with uninjected controls, suggesting that the surgery and vector expression were well tolerated (Figure S4).

Clrn1 delivery with AAV-S rescues morphology of hair bundles and auditory nerve fibers in the *TgAC1*$^{+}$*/ClrnKO* mouse model of Usher 3A

To better understand the AAV-S-mediated rescue of hearing, we performed scanning electron microscopy at P60 and P150 in untreated wild-type and $TgAC1^{+}/Clrn1KO$ mice and in mice treated at P1 with 1.9×10^{10} VG of AAV-S-optiClrn1. Scanning electron microscopy revealed that wild-type C57BL/6J mice had well-organized hair bundles in IHCs and OHCs (Figures 3C and 3D). In untreated $TgAC1^{+}/Clrn1KO$ mice, both IHC and OHC hair bundles showed a loss of short-row stereocilia (Figure 3C′, black arrow) at P60, and some hair bundles were missing entirely (Figure 3C′, white asterisk). The degeneration progressed: whereas wild-type mice showed good bundle morphology at P150 (Figure 3D), most hair cells were gone by P150 in $TgAC1^{+}/Clrn1KO$ mice (Figure 3D′), with just a few patches of

Figure 2. AAV-S efficiently transduces multiple cell types in the neonatal mouse cochlea

(A) Schematic of the cochlea, with described regions numbered (see Table 1). Colored lines indicate the location of optical sections in the panels below. (B–H, J, and J′) Representative confocal images of whole-mount cochleas. C57BL/6J mice were injected via the round window membrane with AAV-S-CBA-EGFP at P1 with 3×10^{10} VG, and the cochleas were dissected and mounted at P6 (n = 8). (B) Confocal images of the apical, middle, and basal regions of the organ of Corti. The upper panel shows EGFP expression (green); the middle panel shows anti-MYO7A labeling for inner and outer hair cells (magenta), and the lower panel is a merged image. (C and D) Cochlea immunostained with anti-NF-H (magenta). Nerve fibers of the apical, middle, and basal regions (C) and cell bodies of spiral ganglion neurons (D) were transduced with AAV-S-CBA-EGFP (green, labeled with white asterisks). (E) Transduced interdental cells and fibrocytes of the spiral limbus (green). (F) Lateral wall, including EGFP-positive fibrocytes of the spiral ligament (green). (G) Outer sulcus cells and Claudius cells. Phalloidin labels filamentous actin (magenta). (H) Inner sulcus cells. (I and I′) Transduction efficiency in IHCs (I) and OHCs (I′) in C57BL/6J mice injected AAV-S-CBA-EGFP at P1 with 3×10^{10} VG. Bars indicate mean ± SEM (n = 8). (J and J′) Transduction by AAV-S-CBA-EGFP of hair cells and supporting cells in the macula of saccule; middle panels show anti-MYO7A labeling of hair cells. (J) is a top view; (J′) is a side view. (K) Auditory brainstem response (ABR) and (K′) distortion product otoacoustic emission (DPOAE) in wild-type C57BL/6J mice injected with 3×10^{10} VG of AAV-S-CBA-EGFP at P1. ABR and a DPOAE tests were performed at P25 for vector-injected (green; n = 3) and non-injected (black dashed; n = 3) animals. Bars indicate mean ± SEM. Scale bars, (B)–(H) 20 μm; (J) and (J′) 40 μm.

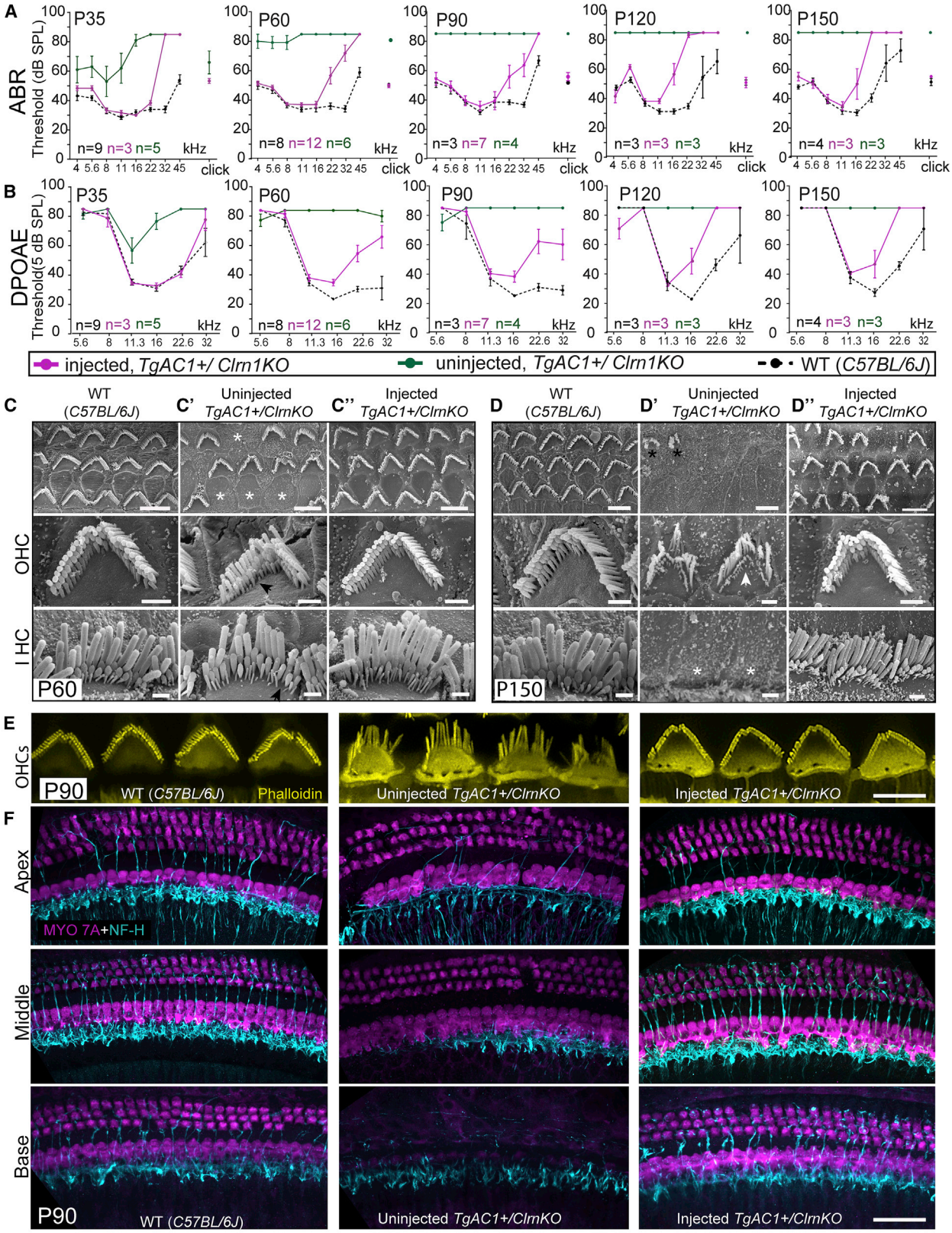

(legend on next page)

surviving OHCs (Figure 3D′, black asterisk). Even those were severely disorganized and showed loss of short- and middle-row stereocilia (Figure 3D′, white arrow). In contrast, *TgAC1*$^{+}$*/Clrn1KO* mice injected with AAV-S-optiClrn1 displayed robust rescue of hair bundle morphology at all tested ages (Figures 3C″ and 3D″).

Phalloidin staining of hair bundle actin also showed that untreated *TgAC1*$^{+}$*/Clrn1KO* mice had disorganized bundles in OHCs, with loss of short and middle stereocilia rows and preservation of only the tallest row (Figure 3E). Similarly, *Clrn1* delivery with AAV-S into *TgAC1*$^{+}$*/Clrn1KO* mice fully rescued the morphology of OHCs, with bundles appearing like those observed in wild-type C57BL/6J mice at P90 (Figure 3E).

We also evaluated innervation of hair cells in treated and untreated animals at P90—an age when untreated *TgAC1*$^{+}$*/Clrn1KO* mice were deaf—using immunofluorescence to observe hair cells with anti-MYO7A and nerve fibers with anti-NF-H. *TgAC1*$^{+}$*/Clrn1KO* mice had a significant loss of auditory nerve fibers across the cochlea and total loss of hair cells in the basal region of the cochlea compared to wild-type controls (Figure 3F). *TgAC1*$^{+}$*/Clrn1KO* mice injected at P1 with AAV-S-optiClrn1 showed no detectible loss of hair cells or nerve fibers compared to wild-type C57BL/6J mice (Figure 3F).

AAV-S mediates efficient transgene expression in the NHP inner ear

While the mouse serves as a convenient species for testing new vectors—especially for measuring phenotype recovery—larger animals such as NHPs provide a much more relevant model for transgene delivery to the human inner ear. Our group has previously reported an effective surgical approach for delivering AAV vectors to the inner ears of cynomolgus monkeys.[5,6] We used this method to test whether AAV-S can transduce the cochleas of NHPs, using the same EGFP reporter cassette as in the mouse. We injected three cynomolgus monkeys (*Macaca fascicularis*; Table S1). The first received AAV-S-EGFP via RMW injection in one ear (5.8×10^{11} VG). For the two other monkeys, we injected two cochleas with another "high" dose (4.7×10^{11} VG), a third with a "low" dose (8×10^{10} VG), and the last with phosphate-buffered saline (PBS). Three weeks post-injection, animals were euthanized. Cochleas were extracted from the temporal bones of animals, further trimmed, and decalcified in 10% EDTA for ~2 weeks. These cochleas were either whole-mounted or embedded in optimal cutting temperature (OCT) compound and cryosectioned. All cochleas were stained with anti-EGFP antibodies, as well as for markers of various cell types.

Anti-EGFP immunostaining at low magnification revealed broad transduction throughout the NHP organ of Corti (Figure 4). Almost all cell types of the cochlea were transduced at the high doses (see schematics in Figures 4F and 5B; linking to Table 1). In particular, we observed a very high level of EGFP expression in the organ of Corti, outer and inner sulcus cells, spiral limbus, lateral wall, and Reissner's membrane (Figures 4A, 4B, and 4E; Video S1). The low-dose (8×10^{10} VG) cochlea showed a greatly reduced transduction efficiency in all cells of the cochlea with the exception of the lateral wall, spiral limbus, and outer sulcus epithelium in the base, which had good transduction (Figure 4C). No specific signal was observed in the cochlea injected with PBS (Figures 4D and S5).

We analyzed higher-magnification images of the organ of Corti from base to apex (Figures 5A and 5C–5C″). In the cochleas administrated with the highest doses (4.7×10^{11} and 5.8×10^{11} VG) the hair cells, Deiters' cells, inner phalangeal cells, pillar cells, Hensen's, and Claudius cells appeared to be completely transduced (Figures 5A–5C′; Video S1). Epithelial cells of the inner sulcus, as well as basilar membrane fibrocytes, were also highly transduced (Figures 5A, 5B, and 5C″). The spiral ligament of the lateral wall revealed significant transduction in fibrocytes (Figures 5D and 5E; Video S2). Notably, high-magnification images from the modiolus region of the cochlea injected with 4.7×10^{11} VG showed high EGFP expression in satellite glial cells and Schwann cells, but almost no transduction of SGNs (Figure S6A). No specific signal was observed in the organ of Corti injected with PBS (Figure S5).

Quantification of vector transduction efficiency in IHCs and OHCs in a cochlea injected with 5.8×10^{11} VG of AAV-S-CBA-EGFP and analyzed with whole-mount imaging showed that at the high dose, AAV-S transduced nearly 100% of both IHCs and OHCs in the apical, mid-apical, and middle regions (Figures 4G and 4G′). The

Figure 3. AAV-S-optiClrn1 delivery robustly and durably rescues hearing and morphology of hair bundles and auditory nerve fibers in the *TgAC1*$^{+}$*/ClrnKO* mouse model of Usher 3A

(A and B) ABR and DPOAE thresholds at P35, P60, P90, P120, P150 of wild-type C57BL/6J mice (black dashed; n = 3–9) and *TgAC1*$^{+}$*/Clrn1KO* mice, either untreated (green; n = 3–6) or treated at P1 with AAV-S-optiClrn1 (1.9×10^{10} VG) (magenta; n = 3–12). Untreated *TgAC1*$^{+}$*/Clrn1KO* mice show some residual auditory sensitivity at P35 that is largely absent by P60. Treated mice retain near-wild-type sensitivity at low and middle frequencies to at least P150. Error bars indicate mean ± SEM. (C) Representative scanning electron micrographs of hair bundles of the cochlea. All images were collected from the mid-cochlear region at P60 or P150. (C and D) Wild-type C57BL/6J mice (n = 3–4). (C′ and D′) Untreated *TgAC1*$^{+}$*/Clrn1KO* mice (n = 3–5). (C″ and D″) Mice treated at P1 with AAV-S-optiClrn1 (1.9×10^{10} VG) (n = 3–4). Missing hair bundles are labeled with white asterisks; surviving but severely disorganized hair bundles are labeled with black asterisks; black arrow points to a loss of short-row stereocilia; white arrow points to a loss of middle-row and short-row stereocilia. Scale bars, upper panels 5 μm; middle and lower panel, 1 μm. (E) Confocal images of OHC bundles at P90 labeled with phalloidin (yellow). Wild-type C57BL/6J mice (left panel, n = 3). Untreated *TgAC1*$^{+}$*/Clrn1KO* mice (middle panel, n = 4). *TgAC1+/Clrn1KO* mice treated at P1 with AAV-S-optiClrn1 (right panel, n = 3). Scale bar, 5 μm. Bundles are disorganized in untreated mutant animals and largely normal with treatment. (F) Confocal images of the apical, middle, and basal regions of whole-mount cochleas at P90 immunostained with anti-MYO7A (magenta) to label hair cells and anti-NF-H (cyan) to label cochlear nerve fibers. Cochlear innervation is markedly reduced in untreated mutant animals (middle panel, n = 4) and retained with treatment (right panel, n = 3). Scale bar, 20 μm.

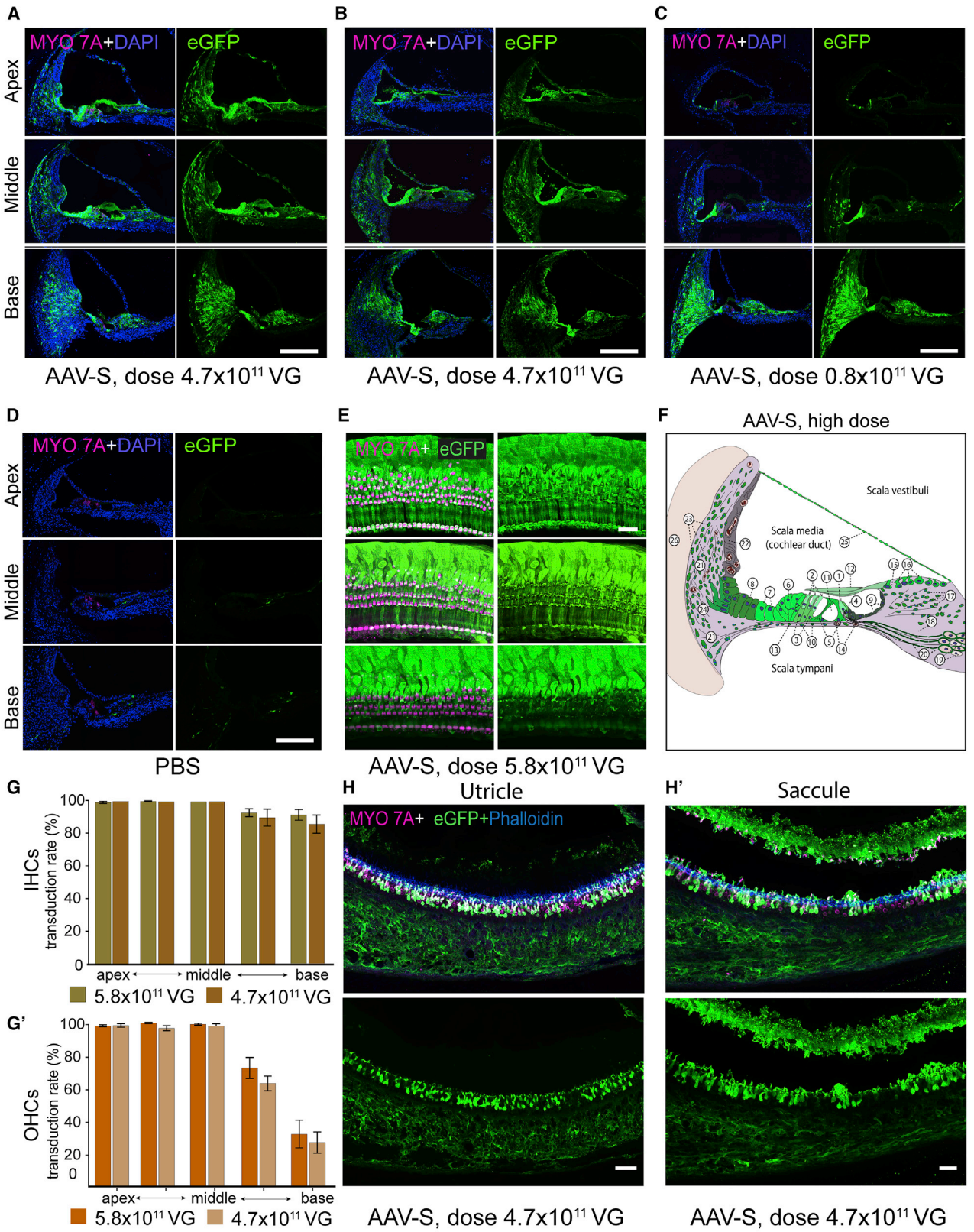

(legend on next page)

transduction remained at 100% in IHCs but showed a decrease in OHCs to 70% in the mid-base region and 30% in the basal region of the cochlea. The same pattern of transduction was observed in ears injected with 4.7×10^{11} VG of AAV-S-CBA-EGFP (Figures 4G and 4G′).

Some forms of genetic deafness also cause vestibular dysfunction. Since the cochlear perilymph is continuous with perilymph that fills the vestibular labyrinth, we wondered whether AAV-S-CBA-EGFP injected via the RWM would transduce vestibular sensory organs in NHPs and could be a useful vector for gene delivery into human vestibular organs. Indeed, immunofluorescence images of frozen sections of vestibular epithelia injected with 4.7×10^{11} VG of AAV-S-CBA-EGFP revealed robust EGFP expression of the saccule and utricle, the vestibular organs sensitive to gravity and linear head movements (Figures 4H and 4H′). Analysis of high-magnification images from the saccule and utricle revealed robust EGFP expression in both type I hair cells (flask-shaped with an enveloping post-synaptic calyx) and type II hair cells (cylindrical with punctate synapses) (Figures 5F and 5F′).

We also analyzed high-magnification images of Scarpa's ganglion (vestibular) neurons in the ear injected with 4.7×10^{11} VG. Labeling was similar to that in spiral ganglion: high EGFP expression in satellite glial cells and Schwann cells with almost no detectable transduction of vestibular neurons (Figure S6B).

Histopathological analysis of NHPs injected with AAV-S-CBA-EGFP

We analyzed hematoxylin and eosin (H&E)-stained frozen tissue sections from injected and uninjected cochleas to assess pathology. Normal tissue morphology and architecture appeared to be preserved in both treated and untreated groups, with no notable abnormalities (Figure 6). We observed slight immune infiltration in treated cochleas (Figure 6A) that was not seen in PBS-injected cochlea (Figure 6B). Specifically, perivascular mononuclear cell infiltration was present in the modiolus region, and not in the organ of Corti, spiral limbus, or lateral wall. This infiltration was focal and did not appear to prevent the expression of EGFP. Minor changes associated with surgery and vector injection and dissection were observed in all cochleas.

ABR test of NHPs injected with AAV-S-CBA-EGFP

ABR thresholds were tested in 4 ears of two cynomolgus monkeys, before and 3 weeks after the injections (Figure 7; Table S1). The pre-injection normal threshold (mean ± SD) for click ABR was 16.2 ± 2.5 dB normal hearing level (nHL); thresholds for 500 Hz, 1,000 Hz, 2,000 Hz, and 4,000 Hz pure tones were 25 ± 4.1, 18.8 ± 4.8, 11.3 ± 2.5, and 13.8 ± 2.5 dB nHL, respectively. We compared pre-injection thresholds to thresholds 3 weeks after injection to assess changes that may be due to the vector. In the PBS-injected cochlea, no difference was seen in the click ABR threshold after injection (Figures 7A–7A″). In the pure tone ABR, there was a small (10 dB) reduction in sensitivity at the two higher frequencies, likely attributable to the injection procedure itself (Figure 7A″).

In the low-dose cochlea (8×10^{10} VG; Figures 7B–7B″), we saw no change in sensitivity in either click or tone ABR, so the injection procedure does not reproducibly cause a loss of sensitivity. Similarly, in one high-dose cochlea (4.7×10^{11} VG; Figures 7C–7C″), there was no systematic change in sensitivity, so the vector seems not to show toxicity. However, in the other high-dose cochlea (4.7×10^{11} VG; Figures 7D–7D″), hearing was lost altogether. Because the same vector dose did not damage hearing in the other cochlea (Figures 7C–7C″), it is unlikely to be a consequence of the vector but may have been due to mastoid surgery complications such as effusion into the middle ear, which can result in transient conductive hearing loss.[14]

DISCUSSION

We tested a novel AAV9 variant, AAV-S, in the inner ears of mice and cynomolgus monkeys and found that it transduces nearly all cell types of the cochlea with high efficiency. Using EGFP as a marker, we found high levels of transduction in hair cells of both the organ of Corti and the vestibular maculas, as well as in different classes of supporting and epithelial cells in mice. To test functional efficacy, we used AAV-S to deliver an optimized *Clrn1* expression cassette to a mouse model of *CLRN1*-related Usher syndrome and found that we could maintain low- and middle-frequency hearing at wild-type levels for at least 5 months post-injection. We also observed preservation of normal hair-cell morphology in the treated animals. Lastly, we showed that AAV-S also mediates extremely high EGFP expression in the cochlea, saccule, and utricle of NHPs, with a transduction profile largely similar to that in the mouse.

Until recently, progress in gene therapy in the inner ear was slow relative to that in other tissues, such as the eye, in part because conventional AAV capsids were not sufficiently effective in transducing all the important cell types in the cochlea. Engineering of novel AAV variants in recent years has produced new vectors with better efficacy

Figure 4. AAV-S mediates robust transgene expression in a variety of cell types in the NHP cochlea and saccule

(A–D) Representative low-magnification images of frozen sections (18 μm thick) of the apical, middle, and basal regions of the cochlea. (A and B) Cochleas injected with 4.7×10^{11} VG (n = 2 ears). (C) Cochlea injected with 8×10^{10} VG (n = 1 ear). (D) Control ear injected with PBS (n = 1 ear). In each, the right panel shows anti-EGFP labeling (green); the left panel also shows anti-MYO7A labeling (magenta) and DAPI labeling (blue) superimposed to visualize hair cells and nuclei. (E) Whole-mount images of the apical, middle, and basal regions of cochlea injected with 5.8×10^{11} VG (n = 1 ear). (F) Summary schematic of AAV-S transduction (green) in the cochlea. Specific regions are numbered (see Table 1). (G and G′) Transduction efficiency in IHCs and OHCs from apex to base in an NHP cochlea injected with 5.8×10^{11} VG (n = 1 ear) and 4.7×10^{11} VG (n = 2 ears) of AAV-S-CBA-EGFP. Error bars indicate mean ± SEM (H and H′) Frozen sections (18 μm thick) of the utricular macula (H) and saccular macula (H′) in an inner ear injected through the RWM with 4.7×10^{11} VG (n = 2 ears). The upper panels show a superposition of EGFP and MYO7A labels, along with phalloidin (blue) to mark actin of the hair bundles. Scale bars, (A)–(D); 200 μm, (E) 30 μm; (H) and (H′) 50 μm.

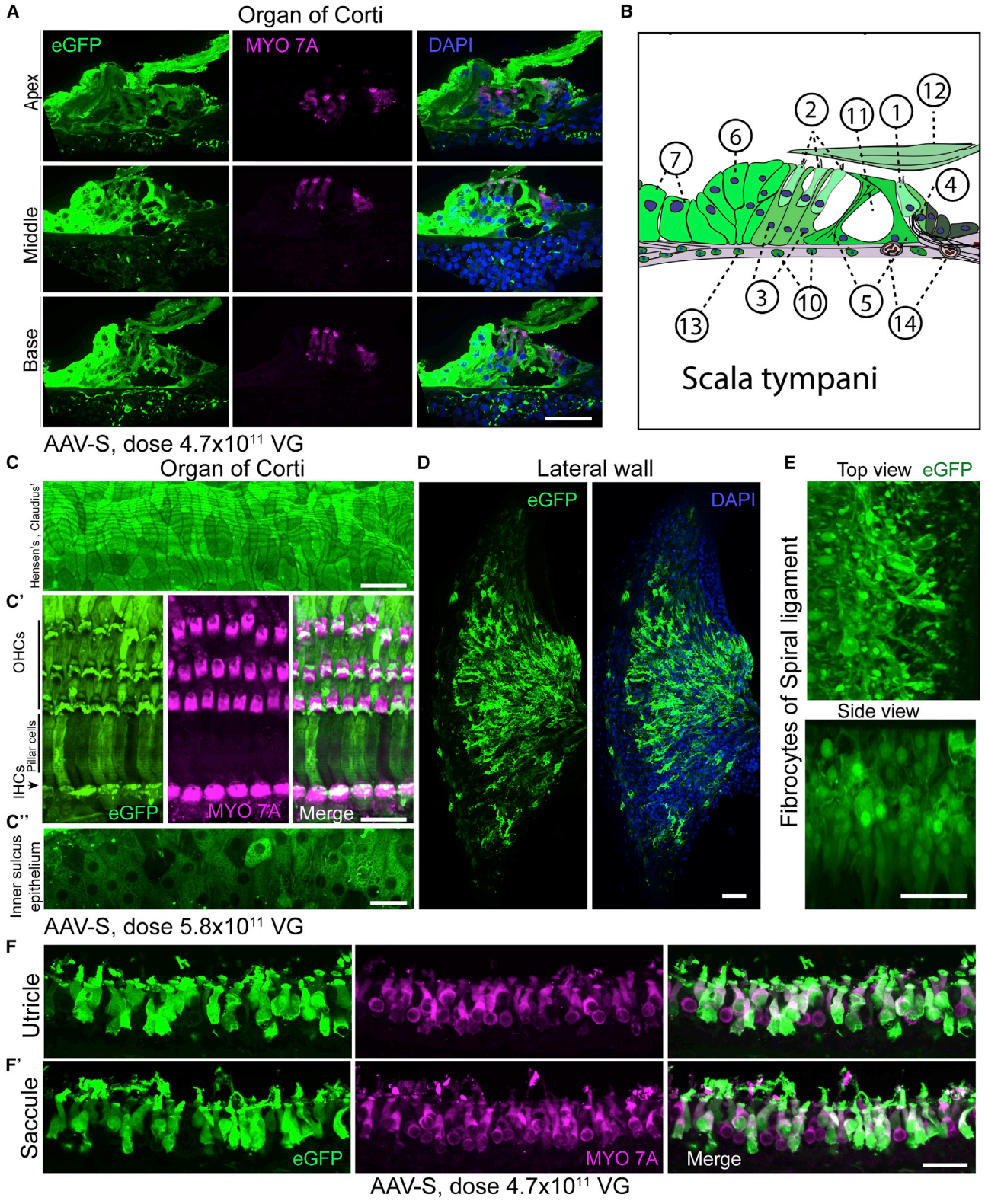

(legend on next page)

in mouse models, especially for cochlear hair cells, including AAV9-PHP.B, AAV2-7m8, and Anc80-L65.[4,5,7–9] Importantly, we have recently shown that, in some cases, vector performance in mouse can translate to larger animals, with the AAV variant AAV9-PHP.B successfully transducing the cochlea of NHPs.[5,6]

However, it will be important to have an array of available vectors as candidates for human gene therapy. Many deafness genes are expressed in hair cells, but some others are not, and vectors should be chosen to optimize tropism. For some genes, off-target expression could be undesirable, so specificity is a consideration. Vector-related immunogenicity is a concern and may vary among serotypes. The true potential of different vectors in different cell types will not be realized until formal toxicology studies and efficacy studies are performed in investigational new drug (IND)-enabling studies with good manufacturing practices (GMP)-grade vector. Thus, a wider pool of available vectors offers a larger tool set for clinical application.

An important test for any vector, beyond expression of a reporter, is treatment of a deafness model. We used AAV-S to deliver an optimized *Clrn1* construct to the *TgAC1-Clrn1-KO* mouse, a model of *CLRN1*-related Usher syndrome type 3A. We found robust rescue of hearing in low and middle frequencies and preservation of hair bundle morphology across all frequencies, up to at least 5 months post-injection (Figures 3A and 3B). The AAV-S-optiClrn1 vector did not rescue hearing at the highest frequencies. This may be a consequence of its more limited ability to express its cargo gene in the high-frequency (basal) OHCs (Figure 2I′). Notably, however, we observed a greater degree of cell survival in the base of treated *TgAC1-Clrn1-KO* mice compared to untreated (Figure 3F), despite the lack of phenotypic rescue. Other AAV variants show a similar inability to transduce high-frequency OHCs and to rescue high-frequency hearing in mouse models of other human deafnesses.[5,15] It is not clear why this is so commonly observed, but we might speculate that it reflects a reduced receptor level or reduced ability to internalize the capsid in basal OHCs (AAV-mediated GFP expression in OHC is lower in the base). Limited high-frequency rescue might also occur if *Clrn1* expression driven by the *Atoh1* promoter is downregulated earlier in the base, which develops earlier, and if vector delivered at P1 expresses *Clrn1* too late to rescue function.

In evaluating AAV-S for clinical use, it was important to assess its ability to transduce a variety of cell types in the NHP inner ear. AAV-S shows a pattern of expression in the NHP mostly similar to that in mouse, with a few exceptions (summarized in Table 1). Curiously, AAV-S did not appear to transduce SGNs in the cynomolgus cochlea (Figure S6) but did in the neonatal mouse (Figure 2D). This is not a simple species difference between mouse and monkey for all AAVs: we found that SGNs in the monkey were transduced by AAV9-PHP.B.[5,6] Thus AAV-PHP.B should be better suited for indications where direct transduction of SGNs is required,[16] and AAV-S for indications in which transduction of SGNs may cause toxicity.

Finally, we tested toxicity of AAV-S encoding EGFP. Histological examination of transduced NHP cochleas showed only focal, minimal infiltration of immune cells, localized in the region surrounding the SGNs, which was not observed in PBS-treated or uninjected animals (Figure 6). This could be a consequence of EGFP expression[6] or of the AAV capsid itself; however, the degree of immune activity observed was minimal.

To assess toxicity, we also tested the hearing of two animals (four cochleas) before and after injection with either AAV-S-EGFP or PBS. In three of four cochleas, the ABR threshold was largely unchanged by the injection. In the PBS-injected cochlea, there was a small (10 dB) reduction in sensitivity at the two higher frequencies. This can be a result of early post-operative changes in the middle ear after mastoid surgery.[14]

In one treated cochlea, however, there was no ABR signal 3 weeks post-injection. There are several possible causes. The transmastoid surgery required to access the cynomolgus RWM is very involved[6] and potentially variable among animals. The ABR threshold shift in this cochlea could be mechanical, from wax in the ear canal or change in middle ear compliance from middle-ear effusion, sometimes observed after mastoid surgery.[14] Vector toxicity is unlikely, as the same vector was well tolerated in two other cochleas (one with equivalent dose), and vector was pre-tested for the presence of endotoxin (<1 EU/mL). The affected cochlea was as effectively transduced as the others and showed no notable pathology in the inner ear (Figure 7). In any case, longer-term toxicology studies using AAV-S encoding clinically relevant transgenes will need to be performed in NHPs to assess indication-specific safety.

In all, we performed a thorough analysis of AAV-S capsid-mediated transduction of the neonatal and adult murine as well as adult NHP cochlea after RWM injection. We found that AAV-S is capable of transducing the majority of cells in the cochlea, and thus it should serve as a useful biological tool for basic inner ear research as well as a promising candidate for inner-ear gene therapy.

Figure 5. Robust transgene expression is observed in the organ of Corti and vestibule in NHPs injected with AAV-S-CBA-EGFP

(A) High-magnification images of frozen sections (18 μm thick) of the apical, middle, and basal regions of the organ of Corti in a cochlea injected with 4.7×10^{11} VG (n = 2 ears). The left panel shows AAV-S-transduced cells, labeled with an antibody to GFP (green); the middle panel shows hair cells labeled with an anti-MYO7A antibody (magenta), and the right panel shows both, along with DAPI labeling of nuclei (blue). (B) Schematic of the organ of Corti. Green indicates EGFP expression mediated by AAV-S. Specific regions are numbered (see Table 1). (C–C″) High-magnification images of a whole mount of a cochlea injected with 5.8×10^{11} VG (n = 1 ear). (C) AAV-S-CBA-EGFP transduces Hensen's and Claudius cells (green). (C′) AAV-S-CBA-EGFP transduces IHCs, OHCs, Deiters', and pillar cells. (C″) AAV-S-CBA-EGFP transduces inner sulcus epithelial cells. (D) The lateral wall of a cochlea injected with a high dose of AAV-S-CBA-EGFP in an 18-μm frozen section. (E) The top view and side view of the spiral ligament, showing labeled fibrocytes. (F and F′) High-magnification images of a frozen section of the utricular macula (F) and saccular macula (F′) in an inner ear injected with 4.7×10^{11} VG. eGFP colocalizes with anti-MYO7A labeling of hair cells, indicating that most hair cells were transduced (white). Scale bars, (A), (D), and (E), 200 μm; (C)–(C″) and (F), 30 μm.

Table 1. Relative transduction efficiency of AAV-S-CBA-EGFP in neonatal and adult mice and NHPs

Region	Cell type	Neonatal mouse	Adult mouse	NHP
Organ of Corti				
1	IHCs	+++	+++	+++
2	OHCs	+++	++	+++
3	Deiters' cells	+++	−	+++
4	inner phalangeal cells	+++	−	+++
5	pillar cells	+++	−	+++
6	Hensen's cells	−	−	+++
7	Claudius cells	++	+	+++
8	outer sulcus cells	+++	+	+++
9	inner sulcus (border) cells	+++	+++	+++
10	fibrocytes of basilar membrane	+++	+++	+++
11	tunnel	−	−	−
12	tectorial membrane	++	+++	+++
13	basilar membrane	−	−	−
14	spiral vessels	nd	nd	nd
15	spiral limbus			
16	interdental cells of spiral limbus	+++	+++	+++
17	fibrocytes of spiral limbus	+++	+++	+++
18	nerve fibers	++	−	−
19	spiral ganglion neurons	+++	−	−
20	glial cells	+++	++	+++
21	lateral wall			
22	stria vascularis	nd	+	+
23	fibrocytes of spiral ligament	+++	+++	+++
24	root cells	nd	nd	+++
25	epithelial cells of Reissner's membrane	+++	+++	+++
26	bone			
Saccule and utricle				
	vestibular hair cells	+++	++	+++
	vestibular supporting cells	+++	+++	−
	Scarpa's ganglion neurons	+++	−	−
	glial cells	+++	++	+++

CBA is a broadly active promoter. Efficiency graded as follows: −, <1%; +, 1%–20%; ++, 20%–50%; +++, >50%; nd, not determined.

MATERIALS AND METHODS

AAV vector production, purification, titration, and endotoxin testing

An AAV plasmid carrying a single-stranded EGFP cassette was used as previously described.[5] EGFP was driven by a hybrid cytomegalovirus immediate-early enhancer/chicken beta-actin (CBA) promoter and contained a woodchuck hepatitis virus post-transcriptional regulatory element (WPRE) and SV40 and bovine growth hormone (BGH) poly(A) sequences, flanked by AAV2 inverted terminal repeats (ITRs).

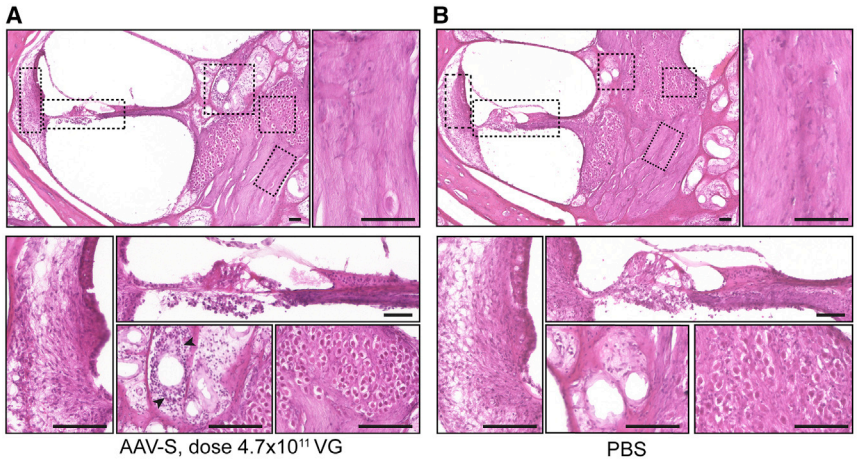

Figure 6. NHPs injected with AAV-S-CBA-EGFP show minimal immune infiltration in the inner ear
(A) Hematoxylin and eosin-stained sections of a NHP cochlea injected with 4.7×10^{11} VG of AAV-S-CBA-GFP. Minimal focal perivascular mononuclear cell infiltration was observed (black arrows). (B) Hematoxylin and eosin-stained sections of a NHP cochlea injected with PBS. Scale bars, 50 μm.

The clarin-1 AAV expression construct (optiClrn1) contained a short (172 bp) 5′ UTR, a mouse codon-optimized *Clrn1* coding sequence (isoform 2), and a long (2.1 kb) 3′ UTR (similar to the construct design by Geng et al.[13]). Expression was driven by a CBA promoter, and the construct contained a BGH poly(A) sequence.

AAV production was performed as previously described.[6] In brief, 293T cells were triple transfected (calcium phosphate method) with (1) AAV rep/cap plasmid encoding AAV2 rep and AAV9 capsid sequence with the AAV-S peptide insert immediately following the nucleotide trio encoding amino acid 588 of VP1; (2) an adenovirus helper plasmid, pAdΔF6; and (3) the AAV expression plasmid with the ITR-flanked transgene expression cassette. Cell lysates were harvested 68–72 h post-transfection and purified by iodixanol density gradient ultracentrifugation. Iodixanol was removed and buffer exchanged to PBS using Zeba desalting columns, 7 kDa molecular weight cutoff (MWCO; Thermo). Vector was concentrated from 4 mL to approximately 100 μL using 2 mL Amicon Ultra 100 kDa MWCO ultrafiltration devices. Vector titers in VG/mL were determined by Taqman qPCR in an ABI Fast 7500 real-time PCR system (Applied Biosystems) using probes and primers to the BGH poly(A) signal and an AAV plasmid standard curve. Endotoxin levels of AAV preparations used in NHP experiments were determined using an Endosafe nexgen-PTS instrument and Endosafe LAL cartridges (Charles River Laboratories). All vector preparations used in NHP studies contained < 1.0 EU/mL. Vectors were pipetted into single-use aliquots and stored at −80°C until use.

Mouse breeding and housing

Animal handling, breeding, and all procedures were performed in compliance with NIH ethics guidelines and with a protocol approved by the Animal Care Committee of Harvard Medical School (HMS). Mice were housed and bred at the HMS animal facility. In this study, C57BL/6J mice were used as the wild-type mice, and all the wild-type control material was obtained from this genetic background. C57BL/6J P1 pups were used for AAV-S-CBA-EGFP transduction experiments. *TgAC1*$^{+}$*/Clrn1KO* mice were a generous gift from Dr. Kumar Alagramam (Case Western Reserve University). Genotyping was done as previously described.[13]

Neonatal mouse RWM injection

The RWM injections were performed under a stereomicroscope (Nikon SMZ1500). P1 pups were anesthetized using hypothermia by exposure on ice and then kept on an ice pack during the procedure. Injections were done via the RWM as previously described.[4] For EGFP expression experiments, 1.5 μL of AAV-S-CBA-EGFP vector solution (3×10^{10} VG) was injected with a micropipette needle at a rate of 150 nL/min using a Nanoliter 2000 Injector (World Precision Instruments). For Clrn1-mediated rescue experiments, 1.2 μL of AAV-S-optiClrn1 vector solution (1.9×10^{10} VG) was injected with a micropipette needle at a rate of 60 nL/min. Standard postoperative care was applied after the injection.

Adult mouse posterior canal (PSC) injections

Adult mouse PSC injections were done as described previously by Suzuki et al.[12] with modifications. C57BL/6J P21 mice were anesthetized with ketamine (100 mg/kg) and xylazine (10 mg/kg) through intraperitoneal injection. GenTeal lubricant eye gel was applied to protect the cornea. After the fur behind the left ear was shaved, the surgical area was cleansed with an antiseptic solution. The area was isolated with sterile drapes and swabbed along the proposed incision with 10% povidone-iodine. A 10- to 15-mm postauricular skin incision was made. After exposing the facial nerve and the sternocleidomastoid muscle by blunt dissection, the tissue covering the temporal bone was retracted. A small 35G hole was made in the PSC, and then a 35G blunt needle was inserted into the opening. A viral suspension of AAV-S-CBA-EGFP (1.5 μL; dose 3×10^{10} VG) at 150 nL/min was injected using the Nanoliter 2000 Injector (World Precision Instruments). The hole was filled in with tissue and sealed with glue. The wound was closed with 7-0 vicryl-coated sutures and swabbed with 10% povidone-iodine. The mouse was placed on a heating pad until full recovery. Animals received an intraperitoneal injection of meloxicam (5 mg/kg body weight) after surgery and once more within the first 24 h. Injected mice were checked daily for 5 days following surgery.

Mouse cochlear histology and imaging

In experiments where transduction efficiency of AAV-S-EGFP was detected via its intrinsic fluorescence, organ of Corti explants or utricle and saccule were dissected at P6 in L-15 medium and fixed with 4% formaldehyde in Hank's balanced salt solution (HBSS) for 1 h, washed three

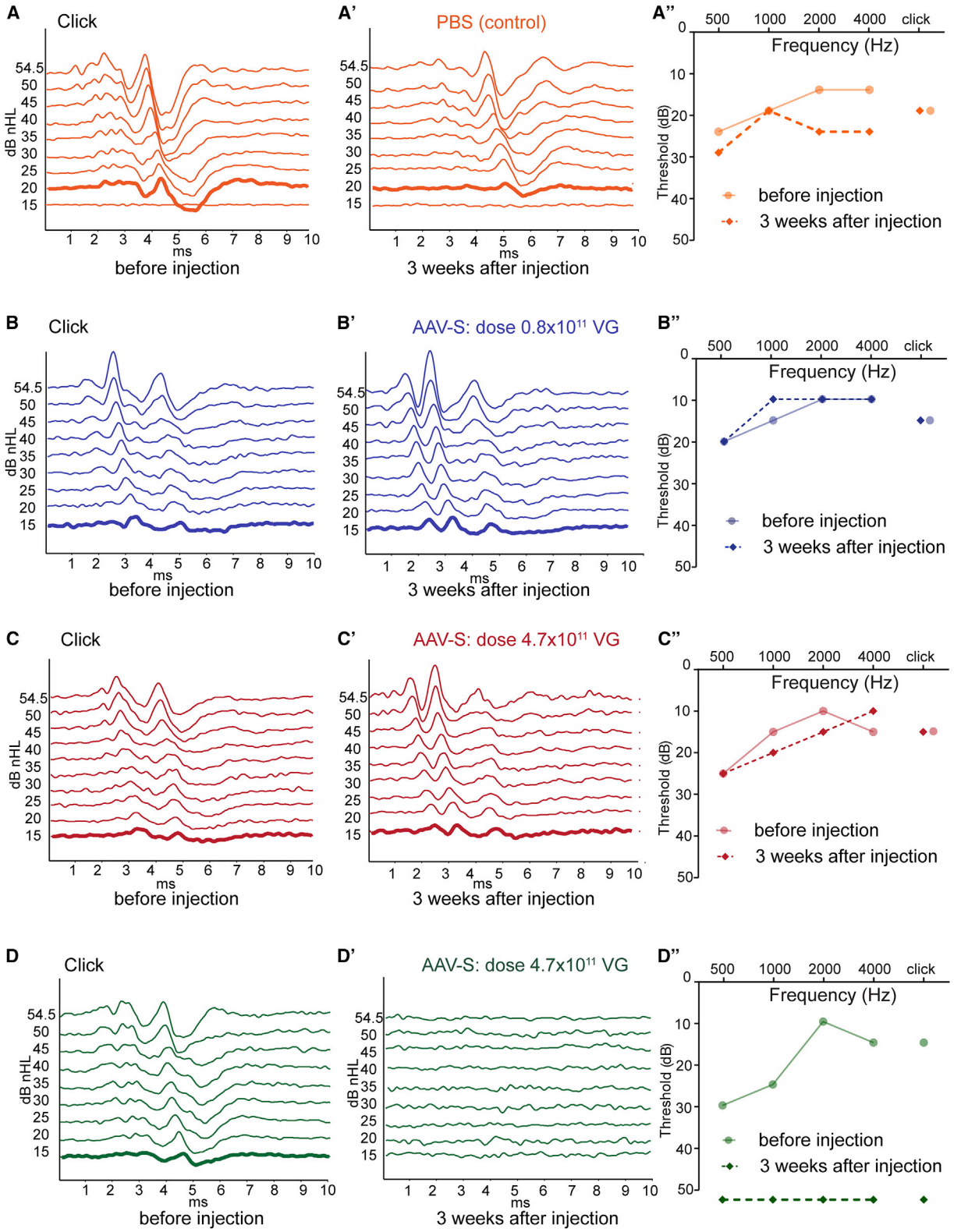

(legend on next page)

times with HBSS, and then blocked and permeabilized with 10% donkey and 10% goat serum with 0.3% Triton X-100 for 1 h at room temperature. Rabbit polyclonal anti-MYO7A antibody (Proteus Biosciences) was used to label hair cells, and chicken anti-neurofilament-H antibody (Millipore) was used to label nerve fibers and SGNs. They were diluted 1:500 in 10% donkey/10% goat serum supplemented with 0.1% Triton X-100/PBS and incubated overnight at room temperature followed by several rinses in HBSS. Next, samples were incubated in blocking solution for 30 min and incubated overnight at room temperature with a donkey anti-rabbit immunoglobulin G (IgG) secondary antibody conjugated to Alexa Fluor 593 in a 1:500 dilution in blocking solution or with a goat anti-chicken IgG secondary antibody conjugated to Alexa Fluor 593 in a 1:500 dilution in blocking solution. To label hair bundle actin, we used phalloidin conjugated to Alexa Fluor 405 (1:20; Life Technologies).

In experiments where the transduction efficiency of AAV-S-EGFP was assessed in the adult cochlea, the intrinsic EGFP signal was amplified with anti-EGFP antibodies. Dissected in L-15 medium, cochleas were immediately fixed with 4% formaldehyde in HBSS for 1 h at room temperature, then washed with HBSS and transferred to fresh 10% EDTA for 2 days. After samples were fully decalcified, the organs of Corti were microdissected, blocked, and permeabilized with 10% donkey/10% goat serum with 0.5% Triton X-100 for 1 h at room temperature. Samples were then stained with rabbit monoclonal anti-EGFP (Thermo Fisher) and chicken anti-Neurofilament-H (Millipore) antibodies or with rabbit polyclonal anti-MYO7A (Proteus Biosciences) and chicken anti-EGFP (Aves) antibodies. They were diluted 1:500 in 10% donkey/10% goat serum supplemented with 0.1% Triton X-100/PBS and incubated overnight at 4°C temperature followed by several rinses in HBSS. Next, samples were incubated in blocking solution for 30 m at room temperature and incubated overnight at room temperature with a donkey anti-rabbit IgG secondary antibody conjugated to Alexa Fluor 488 and with a goat anti-chicken IgG secondary antibody conjugated to Alexa Fluor 593, or with a donkey anti-rabbit IgG secondary antibody conjugated to Alexa Fluor 593 and with a goat anti-chicken IgG secondary antibody conjugated to Alexa Fluor 488, in a 1:500 dilution in blocking solution. To label hair bundle actin, we used phalloidin-Alexa Fluor 405.

In rescue experiments of *TGAC1*$^{+}$*/ClrnKO* P90 mice, the protocol above was used to assess changes in hair cells and nerve fibers. Rabbit polyclonal anti-MYO7A (Proteus Biosciences) and chicken anti-neurofilament-H (Millipore) antibodies were used at 1:500 dilution. To label hair bundle actin, we used phalloidin-Alexa Fluor 405. Tissues were mounted on a Colorfrost glass slide (Thermo Fisher Scientific) using Prolong Gold Antifade mounting medium (Thermo Fisher Scientific). Imaging was performed with a Nikon Ti2 inverted spinning disk confocal using a Plan Apo λ 20×/0.8 objective, Plan Fluor 40×/1.3 oil objective, Plan Apo λ 60×/1.4 oil objective, or Plan Apo λ 100×/1.45 oil objective.

Quantification of transduction efficiency in neonatal mice

Whole-mount cochleas, immunostained as described, were imaged with a Nikon Ti2 inverted spinning disk confocal using a Plan Fluor 40×/1.3 oil objective. Five different regions (apex, mid-apex, middle, mid-base, and base) along the cochlea were imaged and transduced cells quantified. The laser intensity was chosen based on the specimen with the strongest EGFP signal to prevent fluorescence saturation, and the same settings were then used for each image of a set. The efficiency of IHC and OHC transduction was evaluated by two blinded investigators using the ImageJ program (NIH Image). HCs were identified with immunolabeling for MYO7A. Control samples without AAV were used to exclude autofluorescence. Segments with dissection-related damage were removed from the analysis.

Scanning electron microscopy

Adult mice (P60 and P150) were anesthetized with an intraperitoneal injection of ketamine (100 mg kg^{-1})-xylazine (10 mg kg^{-1}). Mice were decapitated after they no longer responded to painful stimuli. Cochleas were extracted in L-15 medium. The stapes from the oval window was removed and the RWM punctured with fine forceps. Under a stereomicroscope, a small hole was made in the apex of the cochlea using a 27G needle connected to a 1-mL syringe. Cochleas then were immediately fixed with a mixture of 1% glutaraldehyde/4% formaldehyde in 0.1 M cacodylate buffer (pH 7.2), supplemented with 2 mM $CaCl_2$ for 1 h at room temperature. Additionally, samples were gently and slowly perfused with 1% glutaraldehyde/4% formaldehyde solution via the round and oval windows until the solution washed out of the small hole at the apex. Then, samples were postfixed with 2.5% glutaraldehyde in 0.1 M cacodylate buffer (pH 7.2), supplemented with 2 mM $CaCl_2$ for 1 h at room temperature. Samples were rinsed in 0.1 M cacodylate buffer (pH 7.2) and then in distilled water. After peeling cochlear bone with the 27G needle, the organ of Corti was microdissected and the tectorial membrane was pulled out. Then, samples were immersed in a saturated aqueous solution of 1% osmium tetroxide for 1 h in the dark, washed with water, and postfixed with 1% tannic acid aqueous solution for 1 h in the dark. Samples were rinsed in distilled water. The osmium-tannic steps were repeated once more. Samples were rinsed in distilled water, dehydrated in an ascending series of ethanol, and critical-point dried from liquid CO_2 (Tousimis Autosamdri 815). Samples were then mounted on aluminum stubs with carbon conductive tabs and were sputter-coated with 5-nm platinum and observed in a field-emission scanning electron microscope (Hitachi S-4700).

Figure 7. ABR testing of NHPs before and after injection of AAV-S-CBA-EGFP showed no loss of sensitivity for most injections

NHPs were tested with click and tone ABR before AAV-S vector injection or PBS control injection and then three weeks later before euthanasia. (A–A″) Saline injection control (n = 1 ear). (B–B″) Low-dose AAV-S (n = 1 ear). (C–D″) High-dose AAV-S (n = 2 ears). Click ABR raw traces before (A–D) and after (A′–D′) injection. (A″–D″) ABR thresholds in response to pure tones of 500, 1,000, 2,000, and 4,000 Hz and to clicks, before (solid) and after (dashed) injection. ABRs are plotted on an inverted scale as for human audiology, so hearing loss (higher threshold) is shown as down.

ABR and DPOAE testing

ABRs and DPOAEs were recorded using an EPL acoustic system (Massachusetts Eye and Ear, Boston, MA, USA) in an acoustically and electrically shielded room. Adult mice (from P25 to P150) were anesthetized with an intraperitoneal injection of ketamine (100 mg kg^{-1})-xylazine (20 mg kg^{-1}) cocktail and placed on a temperature-controlled heating pad set to 37°C for the duration of the experiment. Acoustic stimuli were delivered via a custom acoustic assembly consisting of two electrostatic drivers as sound sources and a miniature microphone at the end of a probe tube to measure sound pressure *in situ*. ABRs were recorded using three subdermal needle electrodes: reference electrode in the scalp between the ears, recording electrode just behind the pinna, and ground electrode in the back near the tail.

For ABRs, 5-ms tone-pip stimuli with a 0.5 ms rise-fall time at frequencies from 5.6–45.2 kHz were delivered in alternating polarity at 30 s^{-1}. The response was amplified (×10,000), band-pass filtered (0.3–3 kHz), and averaged (×512) with a PC-based data acquisition system using the Cochlear Function Test Suite software package (Massachusetts Eye and Ear, Boston, MA, USA). Sound levels were incremented in 5-dB steps, from ~20 dB below threshold up to 80 dB sound pressure level (SPL). ABR Peak Analysis software (v1.1.1.9, Massachusetts Eye and Ear, Boston, MA, USA) was used to determine the ABR thresholds. ABR thresholds were confirmed by visual examination, as the lowest stimulus level in which a repeatable waveform could be observed. DPOAEs were recorded for primary tones (frequency ratio f_2/f_1 = 1.2, level ratio L1 = L2 + 10), where f_2 varied from 5.6 to 45.2 kHz in half-octave steps. Primary tones were swept in 5 dB steps from 10 to 80 dB SPL (for f_2). DPOAE threshold was determined from the average spectra as the f_1 level required to produce a DPOAE of 5-dB SPL.

NHP study design

Three juvenile male cynomolgus monkeys (*Macaca fascicularis*) (1–3 years old, weighing 1.7–3.2 kg) were used in this study. Primate work was performed at Biomere Medical Research Models (Worcester, MA, USA) according to animal use guidelines and approved procedures. Each animal was considered acclimated to the environment at the time of the study. NHPs were healthy and without a history of ear inflammation, ear surgery, signs of balance disorders, or other risk factors for dysfunction of the inner or middle ear. Monkeys received transmastoid/trans-RWM injections of 20 μL of AAV-S-CBA-EGFP with doses of 5.8×10^{10} VG (n = 1 ear), 4.7×10^{11} VG (n = 2 ears), and 0.8×10^{11} VG (n = 1 ear). One animal was injected in one ear with vehicle (PBS) control (see Table S1).

NHP surgical procedures

Pre- and post-operative anesthesia and analgesia

Animals were sedated with ketamine hydrochloride (10 mg/kg) administered intramuscularly and pre-medicated with atropine (0.04 mg/kg) following overnight food deprivation. Prior to surgery, the animals were administered with dexamethasone (1 mg/kg) and buprenorphine (0.03 mg/kg) and received a single dose of buprenorphine sustained-release (SR) (0.2 mg/kg) administered subcutaneously and cefazolin (20 mg/kg). To facilitate induction and intubation procedures, the animals were masked with isoflurane (1%–4%). Animals were intubated and maintained with oxygen (0.5–4 l) and isoflurane (~1%–5%) for the duration of the surgical procedure. Animals received warmed lactated Ringer's solution intravenously (10 mL/kg/h) during the surgery to improve recovery. A non-medicated lubricant was applied to protect the corneas. Hair was clipped from the surgical site, and any loose hair was removed. The surgical injection site was prepared for surgery using a povidone-iodine scrub solution and sponges soaked in 70% isopropyl alcohol. The animals were kept warm throughout the surgical preparation and procedure using warm-water-circulating heating blankets. Heart rate, respiratory rate, blood pressure (as applicable), end-tidal carbon dioxide, and body temperature were continually monitored throughout the procedure and recorded at least every 20 min. The surgical site was prepared for aseptic surgery with a final application of Dura-Prep and allowed to dry prior to sterile draping. Bupivacaine (0.25–0.5 mL per site) was injected subcutaneously for local anesthesia at the incision sites either before the procedure or upon incision closure.

Injection procedure

All viral inner-ear administrations were performed via the facial recess approach, with round-window injection as described.[6] In brief, following a retroauricular incision, the mastoid bone was exposed and cortical mastoidectomy was performed. When the fossa incudis was reached, a 1- to 2-mm facial recess was then identified. A low drill speed and continuous fluid irrigation were used at this area to minimize thermal injury to the facial nerve. Then, the facial recess was opened to approach the RWM.

Under direct visualization through the operating microscope, the needle was manually positioned into the round window and the needle held in place during the infusion. Viral vector injection was performed using a microinjection syringe pump (World Precision Instruments) at 2.0 μL/min for 10 min (for 20 μL total volume), using a Hamilton syringe connected via a thin, relatively non-compliant silicone tube to a 29G, ~2-cm-long, sharp-end stainless steel injection needle. The syringe and catheter were filled with sterile saline and the needle backfilled with 30 μL of vector separated from saline by an air bubble in the catheter.

Once the injection was completed, the surgical site was gently flushed with warm saline. The temporal muscles were approximated with interrupted tension sutures (far-near near-far sutures of 3-0 polydioxanone suture (PDS) followed by continuous subcutaneous and subcuticular sutures of absorbable suture material (4-0 PDS). The skin surrounding the surgical site was cleaned with saline in order and a topical antibiotic ointment was administered to the surgical site immediately after surgery. The surgical wounds were monitored for proper healing daily for 2 weeks.

Postoperative treatment

The animal was allowed to recover from anesthesia and monitored continuously until fully alert. Local anesthesia for the skin incision was achieved using subcutaneous injection of bupivacaine

(0.03 mg/kg) in the evening following surgery (day 0) and twice daily on days 1–3 post-surgery. Dexamethasone (0.5 mg/kg intramuscular) was administrated daily every 8–12 h for up to 5 days after surgery, to reduce fibrosis and inflammatory responses and nausea associated with surgery. Animals received cefazolin (20 mg/kg intramuscular) in the evening following surgery and 3 days later after surgery. Daily wound checks were performed throughout the study. Animals were monitored for evidence of pain and recovery and treated accordingly following completion of the regimen outlined above.

NHP cochlear processing, histology, and imaging

NHPs were euthanized at 21 days after vector injection and were perfused with heparinized saline followed by 4% formaldehyde. Collected temporal bones were postfixed for another 48 h in 4% formaldehyde. Then, cochleas were dissected from the temporal bones under a microscope as described[6] and were transferred to fresh 10% EDTA for 10–15 days until fully decalcified. For whole mounts, cochleas were microdissected and immunostained. For cryosectioning, samples were cryoprotected by incubating in 10%, 20%, and 30% sucrose in PBS and then in NEG-50 (Richard-Allan Scientific) for 2 days, all at 4°C. Cochleas were embedded in NEG-50 and stored at −80°C prior to sectioning. Cryosections were generated using a Leica CM 3050 S cryostat at 20 μm step size. After sectioning, slides were allowed to dry at −80°C overnight.

The same protocol was used for whole-mount immunostaining and cochlear frozen sections. The following primary antibodies and secondary antibodies were used: rabbit polyclonal anti-MYO7A (Proteus Biosciences), mouse polyclonal anti-MYO7A (Proteus Biosciences), chicken anti-neurofilament-H (Millipore), rabbit monoclonal anti-EGFP (Thermo Fisher), chicken anti-EGFP (Aves), donkey anti-rabbit IgG secondary antibody conjugated to Alexa Fluor 593, goat anti-chicken IgG conjugated to Alexa Fluor 488, a goat anti-chicken IgG conjugated to Alexa Fluor 647, donkey anti-mouse IgG conjugated to Alexa Fluor 593, and donkey anti-rabbit IgG conjugated to Alexa Fluor 488.

Samples were blocked and permeabilized with 10% donkey/10% goat serum with 0.3% Triton X-100 for 1 h at room temperature. Anti-MYO7A antibodies were used to label hair cells, anti-EGFP to amplify the EGFP signal, and anti-neurofilament-H to label nerve fibers and SGNs. Antibodies were diluted 1:500 in 10% donkey/10% goat serum supplemented with 0.1% Triton X-100/PBS and incubated overnight at room temperature followed by several rinses in HBSS. Next, samples were incubated in blocking solution for 30 min and incubated overnight at room temperature with secondary antibody in a 1:500 dilution in blocking solution. To label hair bundle actin, we used phalloidin conjugated to Alexa Fluor 405 (Life Technologies) (1:20). We used DAPI to label cell nuclei.

Tissues were mounted on a Colorfrost glass slide (Thermo Fisher Scientific) using Prolong Gold Antifade mounting medium (Thermo Fisher Scientific). Imaging was performed with a Nikon Ti2 inverted spinning disk confocal using a Plan Apo λ 20×/0.8 objective, Plan Fluor 40×/1.3 oil objective, Plan Apo λ 60×/1.4 oil objective, or Plan Apo λ 100×/1.45 oil objective.

For H&E-stained slides, samples were dried at 37°C for 30 min. They were immersed in hematoxylin for 2 m, followed by rinsing in water and destaining with 0.5% hydrochloric acid in 70% ethanol, and rinsed again. Slides were then dipped in eosin for approximately 5 s and rinsed twice each for 1 min in 95% ethanol, 100% ethanol, and xylene. Samples were left to dry and were mounted with SignalStain mounting medium (Cell Signaling Technology). Slides were imaged using a Keyence BZ-X800 microscope, using BZ-Nikon Plan Apo λ 10×/0.45 and Apo λ 20×/0.75 objectives.

Quantification of transduction efficiency in mice and NHPs

Whole-mount cochleas, immunostained as described earlier, were imaged with a Nikon Ti2 inverted spinning disk confocal using a Plan Fluor 40×/1.3 oil objective. Multiple images were taken along the cochlea from apical, mid-apical, middle, mid-basal, and basal regions. The laser intensity was chosen based on the specimen with the strongest EGFP signal to prevent fluorescence saturation, and the same settings were then used for each image of a set. The efficiency of IHC and OHC cell transduction was evaluated by two blinded investigators using the ImageJ program (NIH Image). HCs were identified with immunolabeling for MYO7A. Control uninjected whole-mount NHP samples were used to exclude autofluorescence.

ABR test in NHPs

A hearing test was performed before and 3 weeks after unilateral injection. The monkeys were anesthetized with a mixture of ketamine (10–15 mg/kg) and atropine (0.04 mg/kg). To facilitate induction and intubation procedures, the animal was masked with isoflurane (1%–4%). The animal was then intubated and maintained on isoflurane anesthesia (~1%–5%, oxygen 0.5–4 l). After sedation, hair was clipped and skin cleaned with alcohol. The animals were kept warm throughout the testing procedure using warm-water-circulating heating blankets. Vital signs were monitored. The entire recording procedure generally lasted 40–60 m.

ABRs were acquired using a clinical-grade auditory evoked potential system (GSI Audera v2.7). Scalp potentials were recorded using subdermal needle electrodes applied in a 3-electrode configuration: the positive electrode at the high forehead, the negative electrode above the mastoid ipsilateral to the stimulated ear, and the common electrode at the low forehead at the midline just above the brow ridge. The click and tone pips stimulus were presented at alternate polarity with a tubal insert phone (TIP) 50 GSI generic. The acoustic click was presented at a repetition rate of 11.1 Hz, and waveforms were averaged across 2,004 stimulus repetitions. Clicks were a condensation stimulus of 100-μs duration. Sound levels were incremented in 5-dB steps, from ~15 dB nHL up to 54.5 dB nHL.

Tone frequencies of 500, 1,000, 2,000, and 4,000 Hz were used. The tone pips were presented at a repetition rate of 27 Hz. and waveforms

were averaged across 2,016 stimulus repetitions. Sound levels were incremented in 5-dB steps, from ~10 dB nHL up to 59.5 dB nHL.

GSI Audera v2.7 software was used to determine the ABR thresholds.

Statistics

Statistics was performed using GraphPad Prism. The IHC and OHC cell counting was performed by two blinded investigators using the ImageJ program (NIH Image). The results are shown as mean ± SEM and as indicated in figure legends. Randomization was used whenever possible.

SUPPLEMENTAL INFORMATION

Supplemental information can be found online at https://doi.org/10.1016/j.omtm.2021.03.019.

ACKNOWLEDGMENTS

We greatly appreciate assistance with NHP experiments from Alan LaRochelle at Biomere Biomedical Research Models. We thank Dr. Kumar Alagramam for providing *TgAC1*$^{+}$*/Clrn1KO* knockout mice. We appreciate the use of the Nikon Ti2 inverted spinning disk confocal at the Harvard Medical School MicRoN Microscopy Core and the Hitachi S-4700 scanning electron microscope at the Harvard Medical School Electron Microscopy Facility. We also thank the Neurobiology Imaging Facility (Harvard Medical School), which is supported by the National Institute of Neurological Disorders and Stroke under award number P30-NS072030. We greatly appreciate the help of Pedro Torres de la Marquez (Massachusetts Eye and Ear Infirmary) for his assistance with SWISS-MODEL and Maestro software modeling. We greatly appreciate assistance with laboratory management from Bruce Derfler (Harvard Medical School). We appreciate advice from Vladimir K. Berezovskii (Harvard Medical School; supported by NIH grant P30-EY12196). This work was supported by the National Institutes of Health (R01-DC017117 to C.A.M. and R01-DC016932 to D.P.C) and by a sponsored research agreement from Waypoint Capital, Inc. to C.A.M. and D.P.C.

AUTHOR CONTRIBUTIONS

C.A.M. and K.S.H. conceived of the study. C.A.M., K.S.H., D.P.C., and M.V.I. designed the research study. M.V.I. and K.S.H. performed experiments and analyzed data. D.M.H., A.J.K., C.W.P., Y.L., P.I.T., and J.N. performed experiments. C.A.M. and D.P.C. analyzed data. C.A.M., M.V.I., K.S.H., and D.P.C. wrote the manuscript with input from all of the authors.

DECLARATION OF INTEREST

The authors declare the following competing interests: C.A.M. has financial interests in Chameleon Biosciences, Inc. and Sphere Gene Therapeutics, companies developing enveloped adeno-associated virus vector platform technologies. C.A.M. also has a financial interest in Claritas Bio, a company developing gene therapies to treat hearing disorders. C.A.M.'s interests were reviewed and are managed by the Massachusetts General Hospital and Partners HealthCare in accordance with their conflict of interest policies. D.P.C. has a financial interest in Claritas Bio. C.A.M., K.S.H., D.P.C., and M.V.I. have filed patent applications involving the AAV-S capsid for gene delivery and therapy applications.

REFERENCES

1. Van Camp, G., and Smith, R.J.. Hereditary Hearing Loss Homepage. https://hereditaryhearingloss.org.
2. Delmaghani, S., and El-Amraoui, A. (2020). Inner ear gene therapies take off: current promises and future challenges. J. Clin. Med. *9*, 2309.
3. Yu, Q., Wang, Y., Chang, Q., Wang, J., Gong, S., Li, H., and Lin, X. (2014). Virally expressed connexin26 restores gap junction function in the cochlea of conditional Gjb2 knockout mice. Gene Ther. *21*, 71–80.
4. György, B., Sage, C., Indzhykulian, A.A., Scheffer, D.I., Brisson, A.R., Tan, S., Wu, X., Volak, A., Mu, D., Tamvakologos, P.I., et al. (2017). Rescue of hearing by gene delivery to inner-ear hair cells using exosome-associated AAV. Mol. Ther. *25*, 379–391.
5. György, B., Meijer, E.J., Ivanchenko, M.V., Tenneson, K., Emond, F., Hanlon, K.S., Indzhykulian, A.A., Volak, A., Karavitaki, K.D., Tamvakologos, P.I., et al. (2018). Gene transfer with AAV9-PHP.B rescues hearing in a mouse model of usher syndrome 3A and transduces hair cells in a non-human primate. Mol. Ther. Methods Clin. Dev. *13*, 1–13.
6. Ivanchenko, M.V., Hanlon, K.S., Devine, M.K., Tenneson, K., Emond, F., Lafond, J.F., Kenna, M.A., Corey, D.P., and Maguire, C.A. (2020). Preclinical testing of AAV9-PHP.B for transgene expression in the non-human primate cochlea. Hear. Res. *394*, 107930.
7. Isgrig, K., McDougald, D.S., Zhu, J., Wang, H.J., Bennett, J., and Chien, W.W. (2019). AAV2.7m8 is a powerful viral vector for inner ear gene therapy. Nat. Commun. *10*, 427.
8. Lee, J., Nist-Lund, C., Solanes, P., Goldberg, H., Wu, J., Pan, B., Schneider, B.L., and Holt, J.R. (2020). Efficient viral transduction in mouse inner ear hair cells with utricle injection and AAV9-PHP.B. Hear. Res. *394*, 107882.
9. Landegger, L.D., Pan, B., Askew, C., Wassmer, S.J., Gluck, S.D., Galvin, A., Taylor, R., Forge, A., Stankovic, K.M., Holt, J.R., and Vandenberghe, L.H. (2017). A synthetic AAV vector enables safe and efficient gene transfer to the mammalian inner ear. Nat. Biotechnol. *35*, 280–284.
10. Hanlon, K.S., Meltzer, J.C., Buzhdygan, T., Cheng, M.J., Sena-Esteves, M., Bennett, R.E., Sullivan, T.P., Razmpour, R., Gong, Y., Ng, C., et al. (2019). Selection of an efficient AAV vector for robust CNS transgene expression. Mol. Ther. Methods Clin. Dev. *15*, 320–332.
11. Tao, Y., Huang, M., Shu, Y., Ruprecht, A., Wang, H., Tang, Y., Vandenberghe, L.H., Wang, Q., Gao, G., Kong, W.J., and Chen, Z.Y. (2018). Delivery of adeno-associated virus vectors in adult mammalian inner-ear cell subtypes without auditory dysfunction. Hum. Gene Ther. *29*, 492–506.
12. Suzuki, J., Hashimoto, K., Xiao, R., Vandenberghe, L.H., and Liberman, M.C. (2017). Cochlear gene therapy with ancestral AAV in adult mice: complete transduction of inner hair cells without cochlear dysfunction. Sci. Rep. *7*, 45524.
13. Geng, R., Omar, A., Gopal, S.R., Chen, D.H., Stepanyan, R., Basch, M.L., Dinculescu, A., Furness, D.N., Saperstein, D., Hauswirth, W., et al. (2017). Modeling and preventing progressive hearing loss in usher syndrome III. Sci. Rep. *7*, 13480.
14. Dai, C., Lehar, M., Sun, D.Q., Rvt, L.S., Carey, J.P., MacLachlan, T., Brough, D., Staecker, H., Della Santina, A.M., Hullar, T.E., and Della Santina, C.C. (2017). Rhesus cochlear and vestibular functions are preserved after inner ear injection of saline volume sufficient for gene therapy delivery. J. Assoc. Res. Otolaryngol. *18*, 601–617.
15. György, B., Nist-Lund, C., Pan, B., Asai, Y., Karavitaki, K.D., Kleinstiver, B.P., Garcia, S.P., Zaborowski, M.P., Solanes, P., Spataro, S., et al. (2019). Allele-specific gene editing prevents deafness in a model of dominant progressive hearing loss. Nat. Med. *25*, 1123–1130.
16. Keppeler, D., Merino, R.M., Lopez de la Morena, D., Bali, B., Huet, A.T., Gehrt, A., Wrobel, C., Subramanian, S., Dombrowski, T., Wolf, F., et al. (2018). Ultrafast optogenetic stimulation of the auditory pathway by targeting-optimized Chronos. EMBO J. *37*, e99649.

OMTM, Volume *21*

Supplemental information

AAV-S: A versatile capsid variant for transduction of mouse and primate inner ear

Maryna V. Ivanchenko, Killian S. Hanlon, Daniel M. Hathaway, Alex J. Klein, Cole W. Peters, Yaqiao Li, Panos I. Tamvakologos, Josette Nammour, Casey A. Maguire, and David P. Corey

Table S1. Study design

NHP	gender	age	body weight (kg)	ear	dose	volume	pre- and post-injection ABR
NHP#1	male	3 yr 4 mo	3.0	left	$5.8x10^{11}$ VG	20 μl	Not done
NHP#2	male	1 yr 11 mo	1.7	right	PBS	20 μl	Yes
				left	$4.7x10^{11}$ VG	20 μl	Yes
NHP#3	male	3 yr 8 mo	3.2	right	$4.7x10^{11}$ VG	20 μl	Yes
				left	$8 x10^{10}$ VG	20 μl	Yes

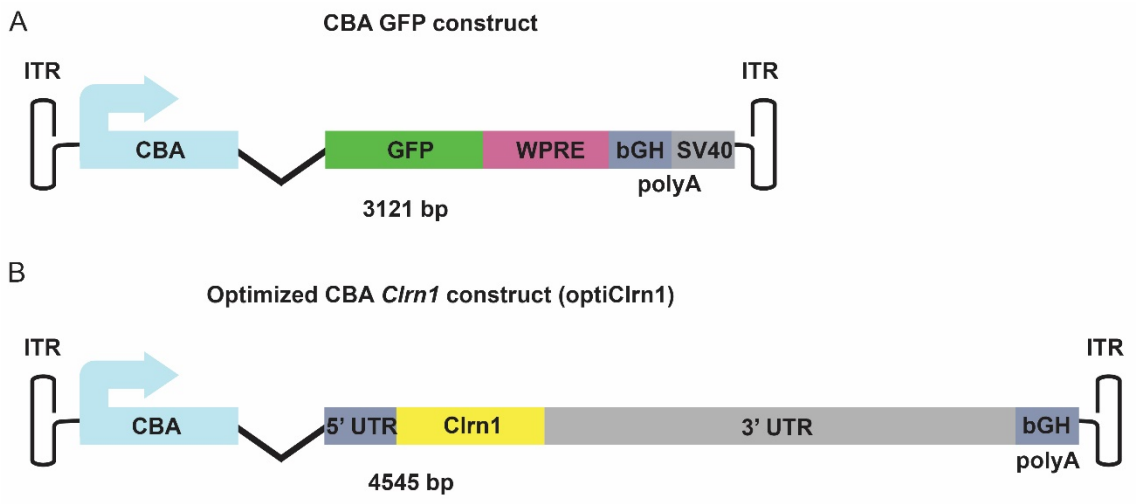

Figure S1. Schematic representation of single-stranded AAV vectors.

(A) AAV eGFP vector. (B) AAV optimized CBA *Clrn-1* vector (optiClrn1).

ITR: inverted terminal repeat

CBA: chicken beta-actin promoter

5'UTR: 5′ untranslated region

3'UTR 3′ untranslated region

WPRE: woodchuck hepatitis virus posttranscriptional regulatory element

pA: BGH poly A signal

Clrn1: mouse *Clrn1* cDNA

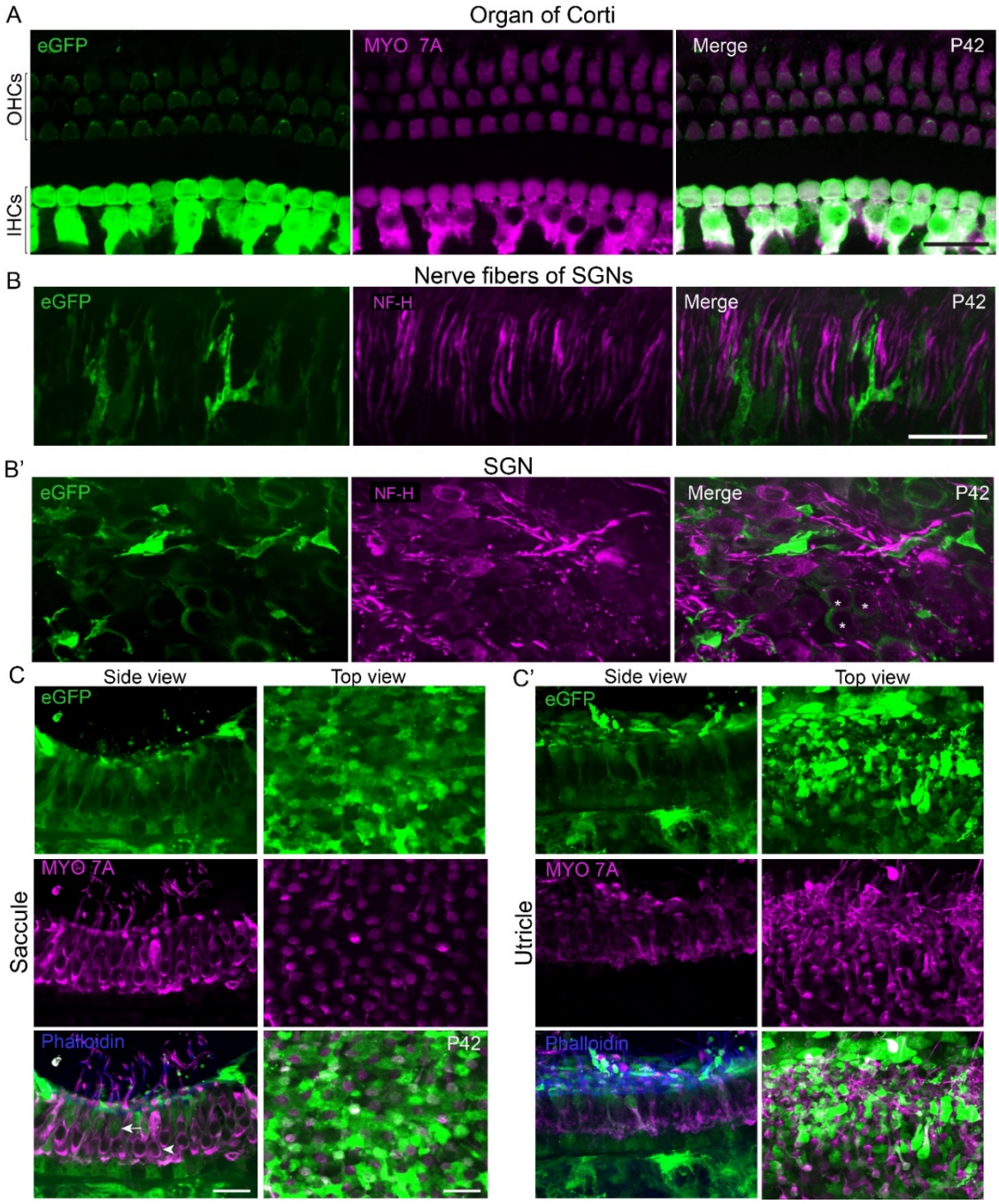

Figure S2. Transduction efficiency of AAV-S-CBA-eGFP in C57BL/6J mice after injection into adult posterior semicircular canal.

(A-C) Confocal images of whole-mount cochlea and saccule. Animals were injected at P21 with AAV-S-CBA-eGFP (3×10^{10}VG) via the posterior semicircular canal and the inner ear was dissected and mounted at P42 (n=4). (A) Confocal images of the organ of Corti of the middle region of cochlea. The left panel shows eGFP expression (green), the middle panel shows an anti-MYO7A labeling (magenta) and the right panel is merged. Inner hair cells are brightly labeled, while outer hair cells are faintly labeled. (B) Cochlea (middle region) immunostained with anti-NF-H (magenta) to show SGN fibers. In adult mouse, nerve fibers show no

transduction. (B') SGN cell bodies also show no transduction, but satellite glial cells and fibrocytes are transduced. (C) Saccular macula, side view (left), Saccular macula, top view (right). (C') Utriclar macula, side view (left), Utriclar macula, top view (right) The right-hand panels show a superposition of eGFP and MYO7A labels, along with phalloidin (blue) to mark actin of the hair bundles. The white arrow points to a transduced hair cell, and the white arrowhead points to an untransduced hair cell. Scale bars: 20 μm.

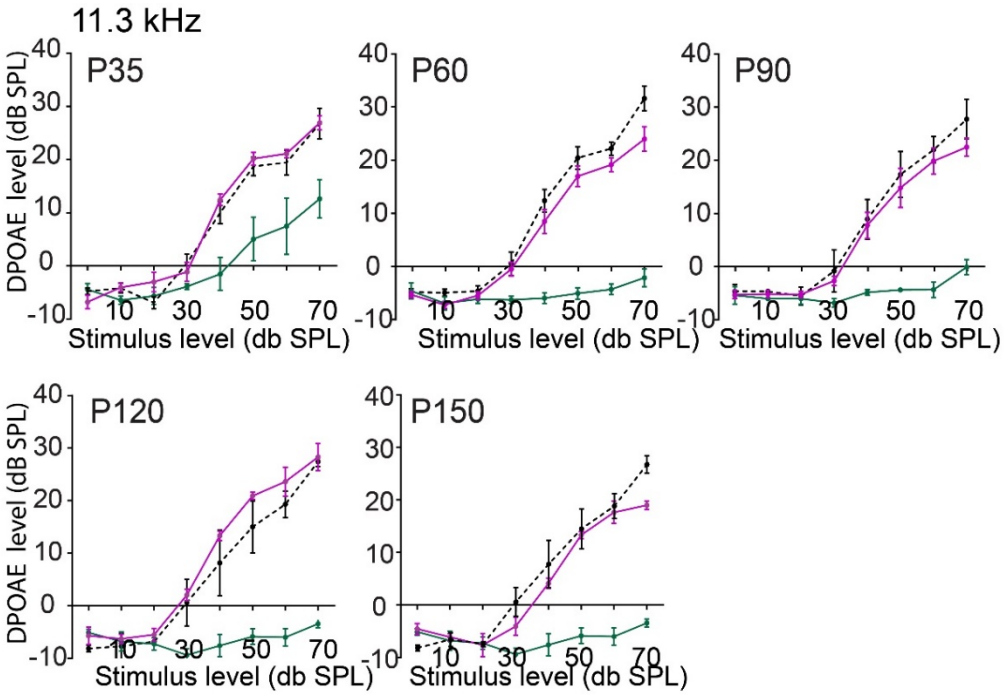

Figure S3. AAV-S-optiClrn1 delivery robustly and durably rescues hearing in the *TgAC1+/ClrnKO* mouse model of Usher 3A. DPOAE amplitudes at frequency 2f1 − f2 (f1/f2 = 1.20) for f2 =11.3 kHz, of wild-type C57BL/6J mice (black dashed; n=3-9) and *TgAC1+/Clrn1KO* mice, untreated (green; n=3-6) or treated at P1 with AAV-S-optiClrn1 (magenta; n=3-12) at at P35, P60, P90, P120, P150. Treated mice retain wild-type sensitivity at 11.3 kHz to at least P150. Bars indicate mean± S.E.M.

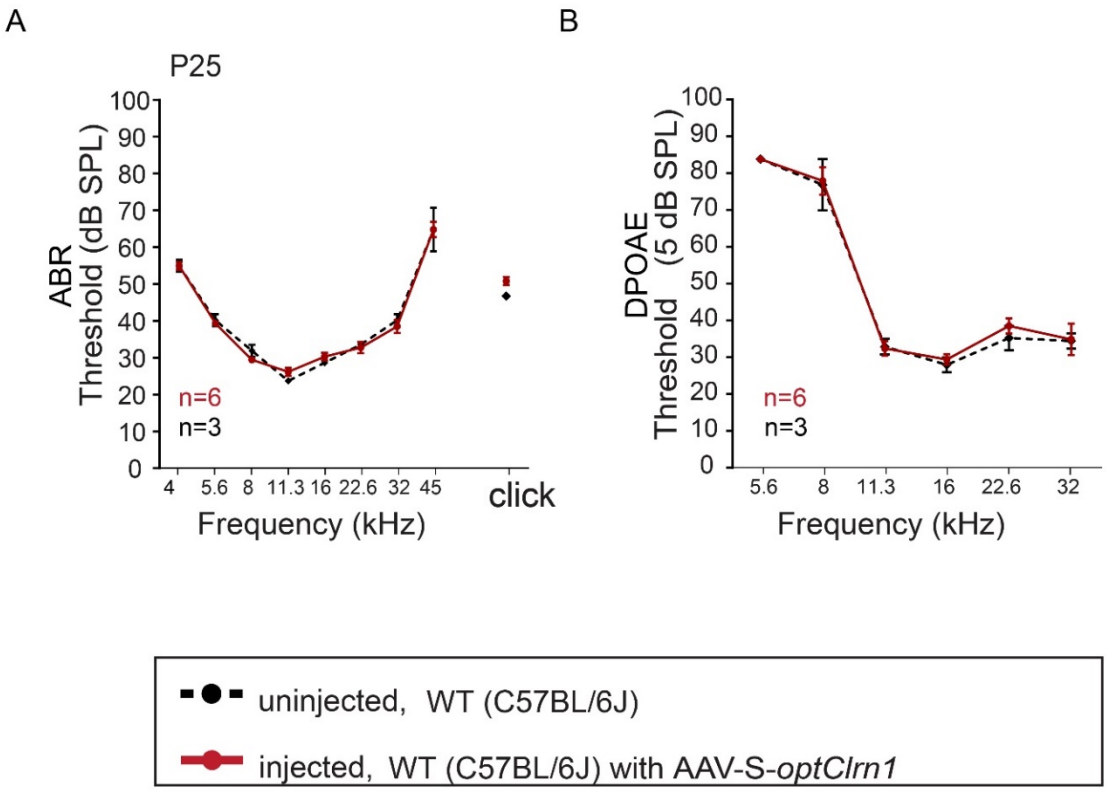

Figure S4. ABR and DPOAE testing of hearing in wild-type C57BL/6J mice injected with AAV-S expressing *Clrn1* and controls. (A) ABR and (B) DPOAE in wild-type C57BL/6J mice injected at P1 with AAV-S-optiClrn1 (3×10^{10} VG). ABR and DPOAE assays were performed at P25 for both vector-injected (red; n= 6) and non-injected (black dashed; n= 3) animals. Error bars indicate mean±S.E.M.

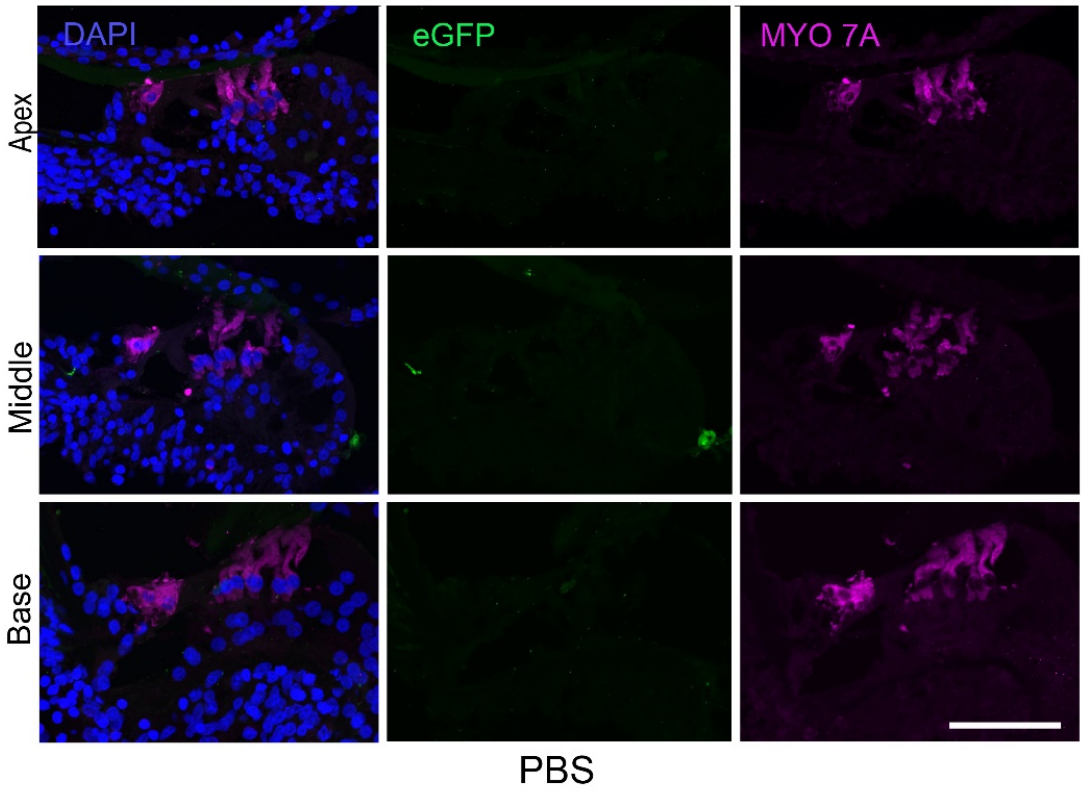

Figure S5. NHP organ of Corti injected with PBS control.

High magnification images of frozen sections (18-μm thick) of apical, middle and basal regions of the organ of Corti in a cochlea injected with PBS. DAPI labels all nuclei, anti-MYO7A labels hair cells. Nonspecific green fluorescence is negligible. Scale bar: 200 μm.

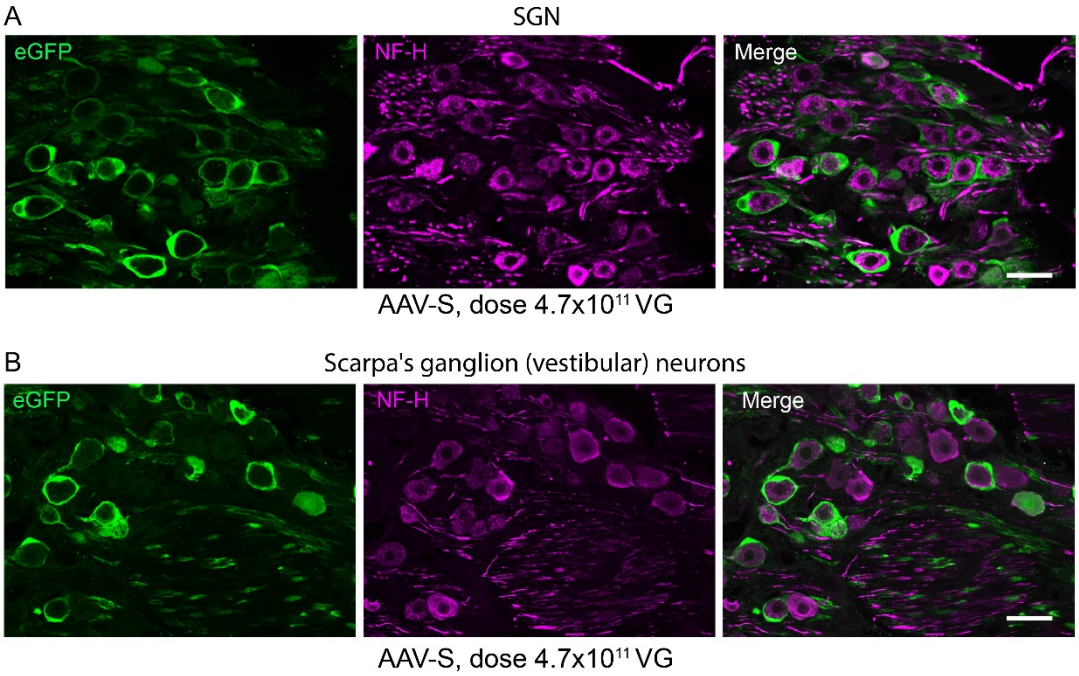

Figure S6. Spiral ganglion and Scarpa's ganglion in an NHP ear injected with AAV-S-CBA-eGFP.

NHP ear injected with AAV-S-CBA-eGFP ($4.7x10^{11}$ VG) and immunostained with anti-eGFP (green) and anti-NF-H (magenta). (A) Spiral ganglion neurons (SGNs) innervating cochlear hair cells. (B) Scarpa's ganglion neurons innervating vestibular hair cells. In NHPs, satellite glial cells and Schwann cells are transduced (green) but apparently not neurons (magenta). Scale bar: 30 μm.

Movie S1. 3D reconstruction of the organ of Corti NHP cochlea injected with $5.8x10^{11}$VG. A 3D reconstruction of the organ of Corti from middle region whole mount NHP cochlea immunostained with anti-eGFP (green), anti-MYO7A (magenta) antibodies, and with phalloidin (blue), at 1.5 µm Z-step using spinning disk confocal microscopy.

Movie S2. 3D reconstruction of the lateral wall NHP cochlea injected with $5.8x10^{11}$VG. A 3D reconstruction of the lateral wall from the middle region whole mount NHP cochlea immunostained with anti-eGFP (green), anti-MYO7A (magenta) antibodies, and with phalloidin (blue), at 1.5 µm Z-step using spinning disk confocal microscopy.